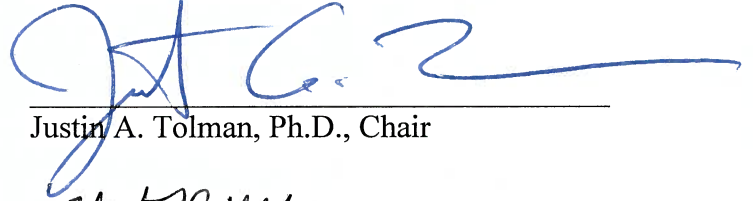


THESIS APPROVED BY

5-6-16
Date



Jeffrey North, Ph.D., Chair



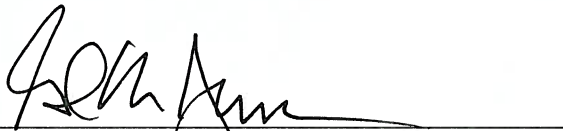
Justin A. Tolman, Ph.D., Chair



Martin R. Hulce, Ph.D.



Alekha Dash, Ph.D.



Gail M. Jensen, Ph.D., Dean

**ANTI-TUBERCULAR CLOFAZIMINE ANALOGS WITH
IMPROVED PHYSICOCHEMICAL PROPERTIES**

**By
Shrouq I. Farah**

A THESIS

**Submitted to the faculty of the Graduate School of the Creighton University in
Partial Fulfillment of the Requirements for the degree of Master of Science in the
Department of Pharmacy Sciences**

**Omaha, NE
(May 2016)**

© Shrouq I. Farah, 2016

ABSTRACT

The worldwide incidence of active tuberculosis (TB) infection was reported to be 9.6 million with the disease responsible for 1.5 million deaths in 2014 despite current treatment approaches that require the use of multiple antimycobacterial agents for extended periods of time. Furthermore, the emergence of the drug-resistant strains has complicated the problem with approximately 190,000 deaths attributed to multidrug-resistant TB (MDR-TB) in 2014. There is a crucial need for the discovery of new anti-TB agents and the reconsideration of older drugs with potent anti-TB activity is a common approach. Clofazimine is an old anti-leprosy agent that has good activity against MDR and extensively drug-resistant (XDR) strains. However, clofazimine's extreme lipophilicity leads to substantial drug accumulation and drug crystallization in body organs and fatty tissues. These crystalline deposits cause gastrointestinal (GI) adverse effects, generalized tissue inflammation, and an undesired reddish-brown discoloration of the skin and conjunctiva. Therefore, structural modifications of clofazimine that would reduce its high lipophilicity while retaining good anti-TB activity would yield an improved anti-TB agent. In this project, the focus was to change the scaffold along with changing two of the substituents. The addition of hydrophilic atoms, such as nitrogen and oxygen, and the removal of lipophilic atoms, such as chlorine, decreased the lipophilicity up to 4000 folds. However, compounds **11**, **13** and **16** were potent against *M. tuberculosis* H37Rv strains with MIC values $\leq 0.8 \mu\text{g/mL}$. Among the three potent compounds, compound **13** had the highest solubility, with a solubility value of $3.66 \mu\text{g/mL}$, the highest permeability, with an apparent permeability (P_e) value of $65.27 \times 10^{-3} \text{ cm/s}$, and the lowest fraction retained in the membrane, with an R value of 0.299. The improved

solubility, permeability and membrane retention suggests that compound **13** is a promising anti-TB agent that has a decreased tendency for lipid accumulation, suggesting improved *in vivo* absorption, distribution and metabolic profile. The anticipated decrease in fat tissue and body organ accumulation is expected to decrease the GI toxicity and discoloration problem which could lead to improved patient compliance.

Dedicated to my God and Lord

ACKNOWLEDGEMENTS

First and foremost, I am ever grateful to God, the Creator and the Guardian, and to whom I owe my very existence, for His blessings that continue to flow into my life and for the strength and knowledge He gave me to continue this research.

I would like to express my deepest gratitude to my advisors, Dr. Justin Tolman and Dr. E. Jeffrey North, for their generous support and encouragement. I have greatly benefited from their guidance, and they both made enormous contribution to my success. I would like to thank Dr. Martin Hulce and Dr. Alekha Dash for being part of my research committee and for their invaluable suggestions. I would also like to express my appreciation for Dr. Somnath Singh for his guidance throughout the Master's program.

I am thankful for St. Jude Children's Research Hospital for performing the MIC studies for clofazimine and the synthesized analogs.

I would personally like to thank Dan Munt for his assistance and advice. Ms. Dawn Trojanowski has been greatly tolerant and supportive along with her administrative help.

A special thanks to my lab members Amruta Sabnis, Rishabh Tukra, Dr. Amit Pandya, Michael Blaha, Ahmed Albariqi, Kyle Graham, Nicholas Franz, Michael Kaminski, Louis Dunn, Kyle Huber, Linh Nguyen and Sristi Singal.

This thesis owes its existence to the help, support and inspiration of my family. I especially thank my hard-working parents who have scarified their lives for me and my siblings. I am also grateful for my husband who has been true and great supporter and has faith in me and my intellect.

Special thanks to the Jack and Lois Wareham Faculty Research Award for funding this project.

TABLE OF CONTENTS

	Page Number
Abstract	iii
Acknowledgements	vi
Table of contents	vii
List of figures	x
List of tables	xii
List of equations	xiv
List of abbreviations	xvi
Chapter 1: Introduction	1
Chapter 2: Design, synthesis and characterization of clofazimine analogs	16
2.1 Clofazimine analogs design	17
2.2 Synthesis and characterization of clofazimine analogs	21
Scheme 1	22
2.3 Conclusion	34
2.4 Experimental	36
2.4.1 Materials and instrumentation	36
2.4.2 Compound synthesis	36
2.4.2.1 Procedure for synthesis of <i>N</i> -(4-chlorophenyl)-3-nitropyridin-2- amine (2)	37
2.4.2.2 Procedure for synthesis of <i>N</i> ² -(4-chlorophenyl)pyridine-2,3-diamine (3)	37

2.4.2.3 Procedure for synthesis of N^2 -(4-chlorophenyl)- N^3 - (5-fluoro-2,4-dinitrophenyl)pyridine-2,3-diamine (4)	38
2.4.2.4 General procedure for synthesis of N^2 -(4-chlorophenyl)- N^3 - [5-(arylamino)-2,4-dinitrophenyl]pyridine-2,3-diamines (5-7)	38
2.4.2.5 General procedure for the synthesis of 10-(4-chlorophenyl)-8- imino- N -(aryl)-8,10-dihydropyrido[2,3- <i>b</i>]quinoxalin-7-amines (11-13)	39
2.4.2.6 General procedure for the synthesis of 10-(4-chlorophenyl)- N - (aryl)-8-(2-propylimino)-8,10-dihydropyrido[2,3- <i>b</i>]quinoxalin- 7-amines (14-16)	41
Chapter 3: Activity and physicochemical characterization of synthesized clofazimine analogs	43
3.1 The new scaffold is active	44
3.2 Clofazimine analogs have lower Clog P values	45
3.3 Clofazimine and its analogs can be quantified using a validated method on UPLC	48
3.3.1 Standard curve	49
3.3.2 Accuracy	52
3.3.3 Precision	53
3.4 The synthesized compounds have improved solubility	55
3.5 The synthesized analogs are more permeable than clofazimine	58
3.6 Conclusion	61
3.7 Experimental	65
3.7.1 Materials and instrumentation	65

3.7.2	UPLC quantification method validation	66
3.7.3	MIC determination	66
3.7.4	Thermodynamic solubility determination	67
3.7.5	Kinetic solubility determination	67
3.7.6	Permeability determination	68
Chapter 4: Conclusion and future perspectives		69
4.1	Conclusion	70
4.2	Global perspectives	72
4.3	Future perspectives	72
4.2.1	Synthetic scheme optimization and synthesis of more compounds	72
4.2.2	Efficacy and pharmacokinetic studies for compound 13	77
4.2.2.1	<i>In vitro</i> intracellular activity study design	77
4.2.2.2	<i>In vivo</i> safety and pharmacokinetic testing study design	77
4.2.2.3	<i>In vivo</i> efficacy study design	78
References		80

LIST OF FIGURES

		Page number
Figure 1	Ideal properties of a novel anti-tuberculosis agent	5
Figure 2	Clofazimine chemical structure	7
Figure 3	A: Deletion of ring A (MIC of 18.89 μ M). B: Deletion of ring D (MIC of > 42.45 μ M). C: Deletion of ring E (MIC of 21.23 μ M)	10
Figure 4	Clofazimine pharmacophore, 5-phenyl-3-imino-phenazin-2-amine	11
Figure 5	Maintenance of the pharmacophore geometric arrangement in scaffold hopping	12
Figure 6	GABA ligands binding to benzodiazepine binding site as a successful example for scaffold hopping	12
Figure 7	Clofazimine SAR based on R1, R2 and R3 substitution	14
Figure 8	Modification of the clofazimine core structure by adding a nitrogen atom to ring A (highlighted purple)	17
Figure 9	R1 substitution with an isopropyl or a hydrogen	19
Figure 10	R ₂ substitution with 4-chlorophenyl, 3-pyridine, and 2-hydroxy-3-pyridine	20
Figure 11	Nucleophilic aromatic substitution reaction mechanism for the coupling of ring A and ring D	24
Figure 12	Nucleophilic aromatic substitution reaction mechanism for the addition of ring C	26
Figure 13	Nucleophilic aromatic substitution reaction mechanism for the addition of ring E	27

Figure 14	The mechanism of the spontaneous cyclization reaction	31
Figure 15	The mechanism of isopropyl amine addition	33
Figure 16	Final products 11–16	35
Figure 17	Absorbance vs. time plot of clofazimine at 286 nm	48
Figure 18	Clofazimine UV absorbance spectrum	49
Figure 19	Clofazimine concentration vs. the area of the absorbance curve at 286 nm	51
Figure 20	Clofazimine concentration vs. the area of the absorbance curve at 492 nm	51
Figure 21	Thermodynamic solubility of clofazimine in different solvents (N = 1)	56
Figure 22	Drug passive diffusion from donor to acceptor plates through an artificial membrane in PAMPA setup	59
Figure 23	The correlation between log P and membrane retention	64
Figure 24	Compounds permeability vs. their retention in the membrane	65
Figure 25	Potential substituents for ring E	74
Figure 26	Further A ring modifications	76

LIST OF TABLES

		Page number
Table 1	R ₁ and R ₂ substituents based on the new scaffold for the synthesized analogs	20
Table 2	MIC of clofazimine and the synthesized analogs	44
Table 3	Log P values, calculated using Schrodinger QikProp software, for clofazimine and the synthesized analogs	47
Table 4	Mean of the calculated values of four different concentrations and the percent of the true concentration at 492 nm	52
Table 5	Mean of the calculated values of four different concentrations and the percent of the true concentration at 492 nm	53
Table 6	The mean and the CV of the AUC for both inter-day and intra-day precision at 286 nm	54
Table 7	The mean and the CV of the AUC for both inter-day and intra-day precision at 492 nm	54
Table 8	Kinetic solubility of clofazimine and six different analogs in SLF	57
Table 9	Acceptor, donor and drug equilibrium concentrations of clofazimine and its analogs that have been used for the calculation of the apparent permeability (P _e) and the fraction retained in the membrane (R)	60

Table 10	A summary of MIC, log P, solubility, P_e , and fraction retained in the membrane (R) for clofazimine and the synthesized analogs	62
----------	--	----

LIST OF EQUATIONS

		Page number
Equation 1	Apparent permeability (P_e) calculation	59
Equation 2	Compound retention in the membrane (R) calculation	59

LIST OF ABBREVIATIONS

WHO:	World Health Organization
TB:	Tuberculosis
<i>M. tuberculosis</i> :	<i>Mycobacterium tuberculosis</i>
MIC:	Minimum Inhibitory Concentration
MDR-TB:	Multi-drug resistant TB
XDR-TB:	Extensively-drug resistant TB
FDA:	Food and Drug Administration
MB:	Multibacillary
Clog P:	Calculated log P
GI:	gastrointestinal
ROS:	Reactive Oxygen Species
SAR:	Structure Activity Relationship
SI:	Selectivity Index
CFU:	Colony Forming Units
TLC:	Thin Layer Chromatography
NMR:	Nuclear Magnet Resonance
UPLC:	Ultra High Performance Liquid Chromatography
DFDNB:	1,5-fluoro-2,4-dinitro-benzene
TEA:	Triethylamine
TMS:	Tetramethylsilane
ESI:	Electrospray Ionization

MS:	Mass Spectrometry
<i>m/z</i> :	Mass to charge
DMSO:	Dimethylsulfoxide
THF:	Tetrahydrofuran
Log P:	The log transformed partition coefficient
PDA:	Photo Diode Array
AUC:	Area Under the Curve
LOD:	Limit of Detection
LOQ:	Limit of Quantification
CV:	Coefficient of Variance
USP:	United States Pharmacopoeia
SLF:	Simulated Lung Fluid
PAMPA:	Parallel Artificial Membrane Permeation Assay
PVDF:	Polyvinylidene Fluoride
P_e :	Apparent permeability
R:	Fraction of the compound that is retained in the membrane
PBS:	Phosphate Buffered Saline

Chapter 1

Introduction

The World Health Organization (WHO) declared tuberculosis (TB) a public health emergency in the 1993 due to the high mortality rates despite current treatment options.¹ In 2014, the worldwide incidence of active TB infection was reported to be 9.6 million people with the disease responsible for 1.5 million deaths.² In the United States, a total of 9,412 new active TB cases were reported in 2014.³ The increase in TB incidence raises the concern about the infection and renews the need to investigate the disease pathogenesis and the contributing factors for TB mortality rates.

Mycobacterium tuberculosis (*M. tuberculosis*), first identified by Robert Koch as the causative pathogen for TB,⁴ is easily transmitted from infected to healthy individuals by the inhalation of infectious aerosols containing viable bacilli.⁵ Mycobacteria are classified as facultative intracellular parasites in macrophages. When the bacilli reach the alveolar region of the lung, they are phagocytized by resident macrophages. The majority of these bacilli are destroyed; however, some have ways to escape the phagocytosis process and replicate intracellularly. Before the macrophages die, they release chemokines to recruit other immune cells and, eventually, a granuloma forms. A granuloma is a lesion of fibroblasts, lymphocytes, monocytes, and neutrophils, in which the mycobacteria are unable to multiply due to low oxygen levels, low pH, and the presence of toxic fatty acids, such as arachidonic acid.^{6,7} Mycobacteria remain viable but dormant for extended periods of time, causing the latent infection. However, when the immune function declines, the granuloma is unable to contain the spread of the bacilli. The bacilli replicate uncontrollably and escape the granuloma, leading to the primary/active infection. HIV co-infection, for example, suppresses the immune system and increases the risk of latent TB reactivation by 20-fold.⁸ The bacilli may infect other

macrophages within the lung (active pulmonary TB) or disseminate through the lymphatic system or blood stream to infect the macrophages in the brain, kidneys, bone or other tissues (extrapulmonary TB).⁹⁻¹² Therefore, the therapeutic concentrations of anti-TB agents require elevated intracellular concentrations inside macrophages that should be higher than the minimum inhibitory concentration (MIC). The MIC value is the lowest drug concentration needed to inhibit at least 90% of bacterial growth.

One third of the world's population carries the asymptomatic latent bacterial form,¹³ and are susceptible to disease reactivation with subsequent transmission, further increasing the risk of tuberculosis spreading. In order to target both the active and the latent phases of TB infection, current treatment approaches require the use of multiple antimycobacterial agents for extended periods of time.

The current first-line short-course TB therapy consists of two phases, an intensive phase and a continuation phase. The initial intensive phase consists of a combination of rifampicin, isoniazid, ethambutol, and pyrazinamide for two months clearing the active/replicating infection. The continuation phase consists of a combination of rifampicin and isoniazid for at least four months, which eradicates the latent bacterial form.¹⁴ This regimen suffers from complexity, length of treatment, and high cost, which result in poor patient compliance.¹⁵ Moreover, first-line anti-tubercular agents have a high risk for drug/drug interactions with drugs used for treating chronic diseases, such as anti-HIV and anti-diabetic agents.¹⁶

HIV is a leading predisposition factor for active TB and higher mortality rates are recorded in TB patients co-infected with HIV.^{17,18} Therefore, the compatibility of current

TB with HIV therapy is necessary. The potential for drug/drug interactions with anti-HIV therapy, including the interaction with HIV reverse transcriptase inhibitors, is one of the major drawbacks of the current approaches to treat TB.

Mutations in the chromosomal genes of the bacilli can result in drug-resistant *M. tuberculosis*. Changes to the *M. tuberculosis* gene expression primarily affect the amino acid sequence in the proteins. This prevents drug interaction with its target proteins, prevent the activation of prodrugs, or produce proteins that can inactivate anti-TB agents by chemical structure modifications.¹⁹ Mycobacteria with resistance mutations are generated through sub-therapeutic drug concentrations and affected by inappropriate drug selection, suboptimal treatment regimens, and patient non-compliance.^{20,21} For example, multi-drug resistant TB strains (MDR-TB) are resistant to rifampicin and isoniazid. Extensively-drug resistant TB strains (XDR-TB) are resistant to rifampicin and isoniazid as well as any of the flouroquinolones and at least one of the injectable aminoglycosides, such as kanamycin and amikacin.²² In 2014, MDR-TB accounted for 190,000 patient deaths worldwide.² Moreover, the number of MDR cases increased by 130% in the Russian Federation over the period of 1999-2009.²³

The increasing prevalence of TB resistant strains is a major contributing factor to TB's mortality rate. Additionally, worldwide epidemiological trends project TB to be a leading cause for morbidity and mortality.²⁴ Despite the severity of this infection, very little progress has been made over the recent decades for improvements to TB treatment options. For example, only bedaquiline and delamanid have been approved by the United States Food and Drug Administration (FDA) as new agents for tuberculosis for 40 years, and they are only reserved to be used for the treatment of MDR-TB.²⁵⁻²⁷ There remain

crucial needs for development of new classes anti-TB agents to combat TB infections, and specifically MDR-TB and XDR-TB strains.²⁸

The need for new anti-TB agents is a non-trivial challenge. The ideal anti-TB drug candidate (Figure 1) will reduce pill burden and dosing frequency, shorten treatment time and be available in low price. It is also favorable that the candidates have new mechanisms of action to treat MDR-TB and XDR-TB strains, and have minimal drug/drug interactions with anti-diabetic and anti-HIV agents.²⁹

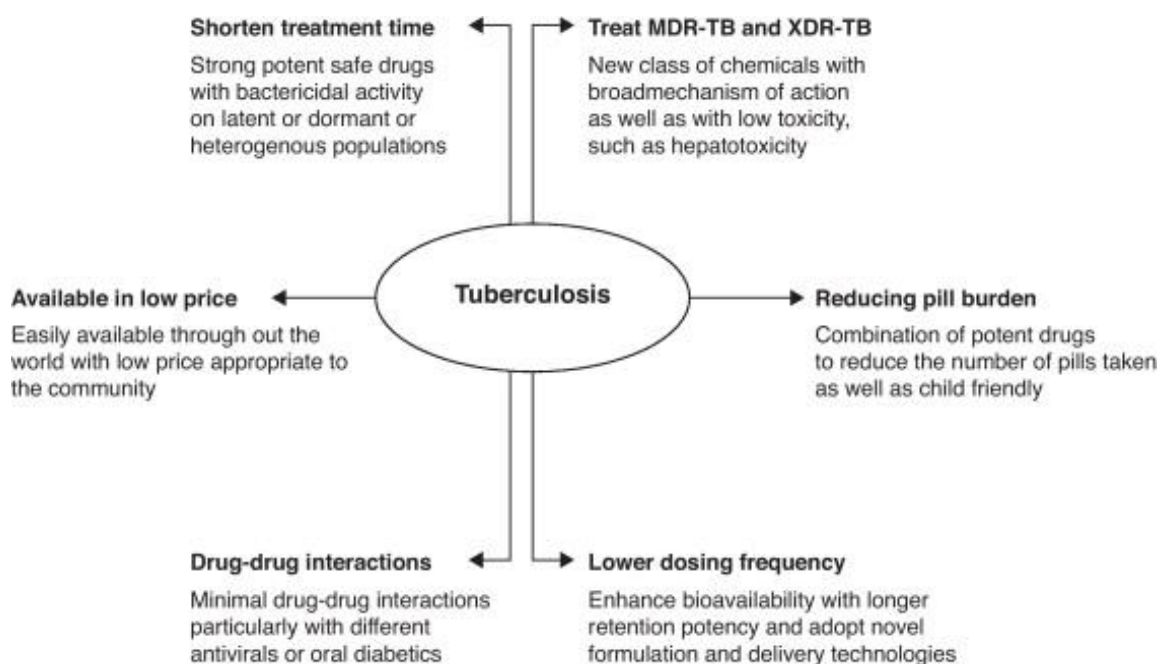


Figure 1. Ideal properties of a novel anti-tuberculosis agent.²⁹

Several approaches have been recently reported in the development of new anti-TB agents. The first major approach is the discovery of active chemical entities by whole cell

screening on viable bacilli followed by the rational drug design that focused on optimization of the active leads through structural modifications. This approach led to the discovery of potent anti-TB agents such as bedaquiline,³⁰⁻³³ delamanid³³⁻³⁶ and PA-824.^{33,37-39} A second major approach is the identification of natural products in attempts to isolate and characterize the active constituents. The natural active constituents can be directly used for TB treatment or modified to afford semi-synthetic potential anti-TB agents.⁴⁰ The third major approach is the reconsideration of older drugs or chemicals that have been found to have good anti-TB activity but are not regularly used clinically due to toxicity or poor pharmacokinetic properties. Linezolid, for example, is an old drug that is found to have good activity against *M. tuberculosis* with MIC range of 0.125 – 0.5 µg/mL.³³ However, in phase I clinical trials, the dose required for TB treatment was found to cause peripheral and optic neuropathy. Structural modifications of these older agents attempt to overcome these limitations and reposition these drugs for regular clinical use for TB therapy.⁴¹

Clofazimine (Figure 2), discovered in 1957 and currently used for multibacillary (MB) leprosy treatment,⁴² is one of the older drugs that has significant activity against TB strains, including MDR-TB strains, with a reported MIC range of 0.12 - 32.00 µg/ml.^{43,44}

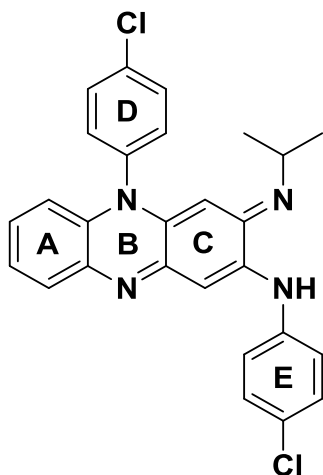


Figure 2. Clofazimine chemical structure.

Clofazimine is chemically identified as N,5-bis(4-chlorophenyl)-3-(1-methylethylimino)-5H-phenazin-2-amine.⁴⁵ It has a phenazine core composed of three aromatic rings (A-C) (Figure 2) with a fourth ring (D) and a fifth ring (E) in resonance with the three-ring core. Clofazimine is considered a riminophenazine since the phenazine is substituted with an isopropyl-imino (R-imino) group. The extended conjugation in the structure is responsible for its red color.⁴⁶ It is a crystalline powder that is insoluble in water with a 2.48 $\mu\text{g/mL}$ aqueous solubility and is highly lipophilic with a calculated log P (Clog P) value of 7.8. Clofazimine's poor aqueous solubility and high lipophilicity lead to substantial drug accumulation and drug crystallization in body organs and fatty tissues. These crystalline deposits cause gastrointestinal (GI) intolerance, generalized tissue and organ inflammation, and an undesired reddish-brown discoloration of the skin and conjunctiva.⁴⁷⁻⁴⁹ These physicochemical properties account for a large volume of distribution of 1470 L⁵⁰ and a long half-life that can be as long as 70 days,^{51,52} which lengthens the time needed for the side effects to wear off. The lipophilic clofazimine weakly inhibits CYP3A4 enzyme without being metabolized, and it is mainly excreted

unchanged in feces.⁵² Inhibition of CYP3A4 is a concern for potential drug/drug interactions with the HIV protease inhibitors, which are metabolized by CYP3A4.⁴⁷

It is controversial that the extreme lipophilicity is needed for clofazimine activity since the exact mechanism of action is still unknown. There are three proposed mechanisms for clofazimine action: (i) production of reactive oxygen species (ROS); (ii) membrane destabilization; and (iii) DNA intercalation. None of these mechanisms has been proven to be true. Nevertheless, it is possible that clofazimine has multiple mechanisms of action and is using all three mechanisms to inhibit mycobacterial growth. The pros and cons of each hypothesis are discussed in the following three paragraphs.

(i) ROS production: clofazimine has a high redox potential and in the presence of oxygen it is likely to be oxidized in the respiratory chain. Clofazimine oxidation leads to the generation of ROS superoxide, $[O_2]^-$, and hydrogen peroxide, H_2O_2 .⁵³ ROS are toxic, interfere with ATP production and ultimately lead to bacterial death. However, clofazimine exposure under anaerobic conditions still has the same inhibitory effect on facultative anaerobic gram-positive bacteria, which means that clofazimine does not need oxygen in its mechanism. Also, the removal of ROS by adding water- and lipid-soluble scavengers and anti-oxidative enzymes does not inhibit clofazimine effect.⁵³ Moreover, 11 different species of Gram-negative bacteria, which are found susceptible to redox cycling mechanism,^{54,55} are found consistently resistant to clofazimine with MIC values > 32 $\mu\text{g/mL}$.⁵³ Thus, the proposed mechanism that clofazimine activity is based on the interaction with the respiratory chain and the production of ROS is unlikely.

(ii) Membrane destabilization: it is hypothesized that clofazimine induces the microbial phospholipases to increase the production of lysophospholipids, agents with membrane-disruptive properties.⁵⁶ Clofazimine and the resulting lysophospholipids interfere with the bacterial phospholipids and prevent K^+ uptake within minutes after exposure, which subsequently destabilizes the membrane, prevents ATP production, and eventually leads to bacterial death.⁵⁶ Lysophospholipids are found in high concentrations in bacterial cells exposed to clofazimine.^{53,56} Additionally, pretreating the bacteria with α -tocopherol, a membrane-stabilizing agent, is able to inhibit clofazimine effect.⁵⁷ These findings along with clofazimine's high lipophilicity support that clofazimine is a membrane destabilizing agent acting on the lipophilic membrane.⁵³ However, phospholipase-deficient mutants have a susceptibility to clofazimine comparable to the standard strains. Therefore, the increased level of lysophospholipids is not attributed to the increased activity of bacterial phospholipases; however it does not exclude the contribution of lysophospholipids in the activity of clofazimine.

(iii) DNA intercalation: There is an evidence that clofazimine binds to bacterial DNA with primary binding sites on the guanine base.⁵⁸ On the other hand, there is no evidence that clofazimine is inserted between the planar base pairs of DNA and local structural changes in bacterial DNA are not seen after clofazimine exposure. Clofazimine is not a mutagenic agent and has high IC_{50} values. Accordingly, these observations indicate that DNA intercalation is an unlikely mechanism of action.

Clofazimine's substantial physicochemical limitations require more than formulation optimization to be an optimal anti-TB agent. Specifically, clofazimine must have structural modifications to improve aqueous solubility and reduce extreme lipophilicity

while retaining good anti-TB activity in order to be an optimum anti-TB agent. Limited reports of chemical modifications to clofazimine analogs have attempted to improve its physicochemical properties, reduce adverse effects, and retain anti-TB activity.^{44,46,59,60}

These preliminary studies identified clofazimine's pharmacophore, which are the structural features essential for activity. Critically, the deletion of rings A, D or E (Figure 3) is detrimental to anti-tubercular activity and results in a significant loss of anti-TB activity (MIC values were increased more than 150-fold over clofazimine).⁴⁶

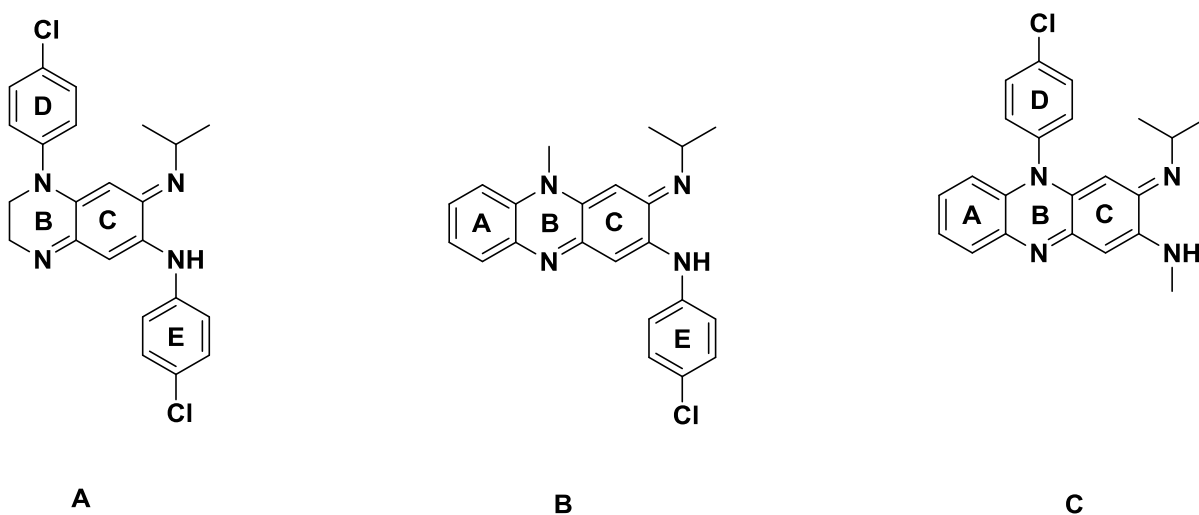


Figure 3. **A:** Deletion of ring A (MIC of 18.89 μM)⁴⁶. **B:** Deletion of ring D (MIC of > 42.45 μM)⁴⁶. **C:** Deletion of ring E (MIC of 21.23 μM)⁴⁶.

This finding suggests that the intact three-ring aromatic phenazine core and two aromatic substituents are essential for activity.⁴⁶ Thus, the clofazimine pharmacophore (Figure 4) is a five-ring structure with extended resonance, and it is hypothesized that changing the scaffold should maintain activity as long as the aromaticity is maintained.

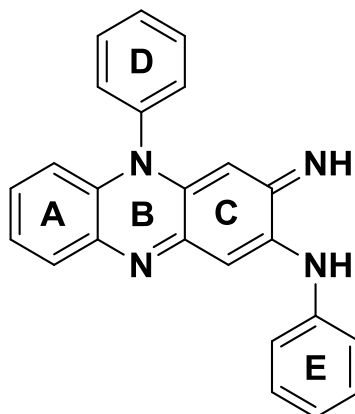


Figure 4. Clofazimine pharmacophore, 5-phenyl-3-imino-phenazin-2-amine.

The term scaffold describes the central core component of a molecule upon which other functional groups are attached. Scaffold hopping is a technique that aims to identify new chemical entities by modifying the scaffold of an active ligand while retaining a specific spatial arrangement of the pharmacophore, which is typically comprised of the attached functional groups (Figure 5). Compounds with the new scaffold are anticipated to have enhanced pharmacokinetic and pharmacodynamic properties while maintaining the same biological activity.⁶¹⁻⁶³

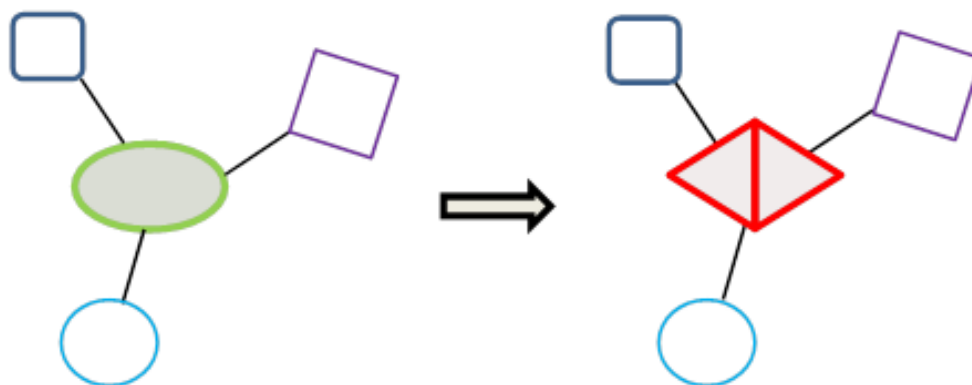


Figure 5. Maintenance of the pharmacophore geometric arrangement in scaffold hopping.

Many drugs currently on the market have been discovered based on the scaffold hopping concept. For example, scaffold hopping helped to enhance the pharmacokinetic and pharmacodynamic properties of diazepam, a benzodiazepine GABA-receptor ligand, and led to the production of the novel compounds zopiclone, zolpidem and zaleplon (Figure 6).⁶⁴

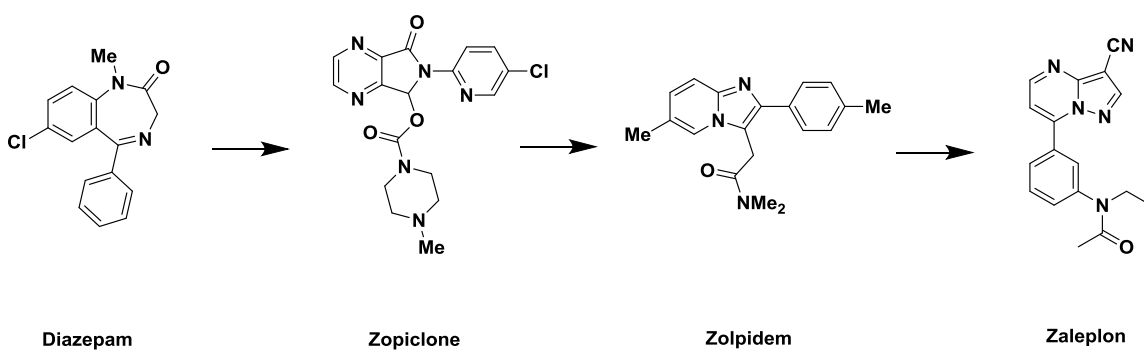


Figure 6. GABA ligands binding to benzodiazepine binding site as a successful example for scaffold hopping.

Although published reports of clofazimine analogs have helped identify the required pharmacophore, there are no reports for scaffold modifications on clofazimine. However, it is anticipated that replacement of clofazimine's scaffold with a more polar three-ring core will maintain the antitubercular activity with improved pharmacokinetic properties.

Structure activity relationships (SAR) were developed through 109 synthesized analogs of clofazimine.^{44,46,59,60} The analogs were tested for their *in vivo* and *in vitro* anti-TB activity, toxicity against mammalian VERO cells, indicated by IC₅₀, selectivity index (SI) and pharmacokinetic properties, such as half-life, C_{max}, and log P. The IC₅₀ value is the concentration of drug required to inhibit 50% of cellular growth. The selectivity index is the IC₅₀/MIC value and, therefore, larger selectivity ratios represent drugs with lower toxicity profiles. Compounds with selectivity indexes greater than 100 are considered excellent and they are expected to have large therapeutic windows.

The summary findings for published studies investigating the SAR of clofazimine have identified three key elements (Figure 7). First, changes to the R₁ position identified that substitution on the imine group with oxygen-containing cycloalkyls maintains antitubercular activity, while substitutions with nitrogen-containing cycloalkyls slightly decrease the activity.⁴⁴ R₁ substitution has a minor impact on activity and, therefore, changing the isopropyl to a more polar substituent is anticipated to decrease lipophilicity and slightly affect activity.

Second, R₂ substitution with a 2-pyridyl group improves the anti-TB activity,⁵⁹ as shown by the more potent MIC value of 0.03 µg/mL⁴⁴ and the drop in the lung bacterial colony

forming units (CFU) by up to 100,000 folds compared to the untreated mice.⁴⁶ R₂ substitution with a pyridyl ring drastically improves activity and, with pyridine being hydrophilic, it is anticipated to decrease the lipophilicity of clofazimine.

Third, R₃ was substituted with halogenated phenyl rings. The results show that the number, position, and type of halogens do not have a significant impact on the activity.⁴⁴ R₃ substitution has a minor impact on activity and because it is synthetically tractable, the improved hydrophilicity by halogen removal can be tested by the removal of the R₂ chlorine, without changing R₃.

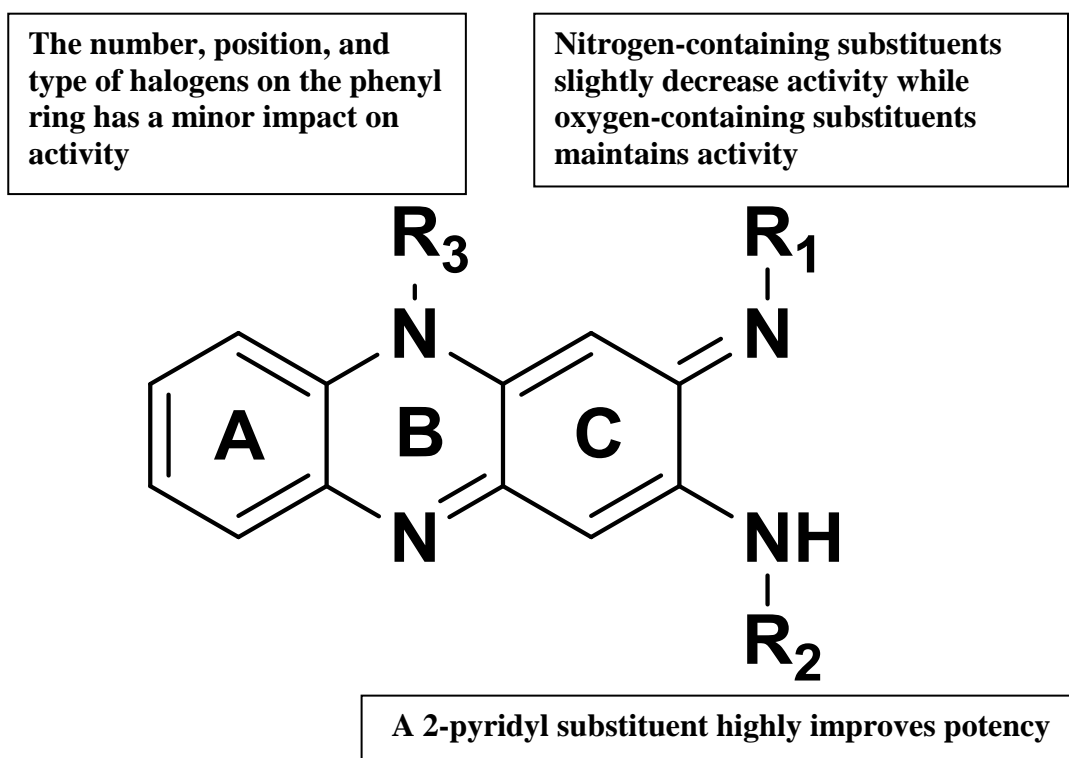


Figure 7. Clofazimine SAR based on R₁, R₂ and R₃ substitution.

It is hypothesized that: **replacing the lipophilic scaffold of clofazimine with a more polar three-ring core in addition to substitutions to R₁ and R₂ will maintain the anti-TB activity while improving solubility and permeability of the analogs.** Improvement of the aqueous solubility and membrane permeability of clofazimine analogs should then eventually lead to toxicity reduction and pharmacokinetic properties improvement of clofazimine analogs compared to clofazimine. Additionally, changes to the three-ring core will lead to a class of novel structures for further explorations into new anti-TB agents.

Chapter 2

Design, synthesis and characterization of clofazimine analogs

2.1. Clofazimine analogs design

The hypothesis was tested by introducing a nitrogen atom to the A ring of the central core structure of clofazimine (Figure 8). The substitution of the phenyl ring with the more hydrophilic pyridine makes the whole scaffold more hydrophilic.

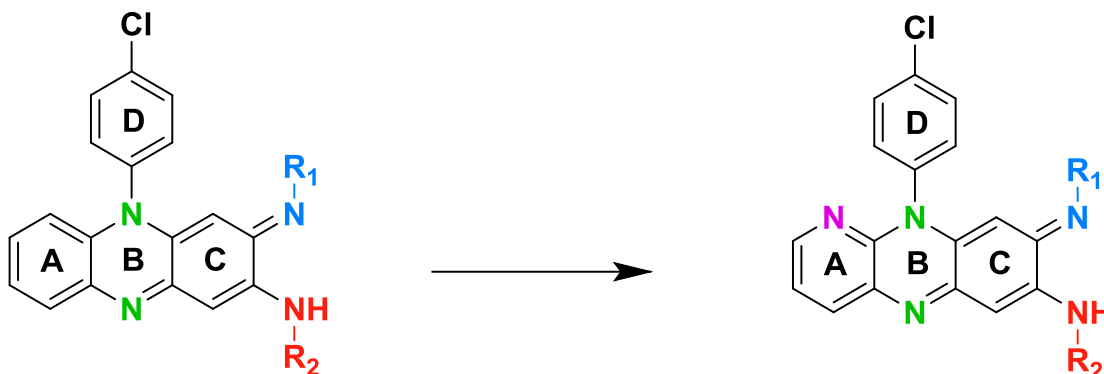


Figure 8. Modification of the clofazimine core structure by adding a nitrogen atom to ring A (highlighted purple).

Pyridine is a more polar bioisostere of a phenyl ring. The bioisosterism concept, originally envisioned in 1909 by James Moir,⁶⁵ refers to the structurally related compounds that are typically recognized in the same way by biological systems. Human protein receptors, for example, are unable to distinguish between O, NH, and CH₂ and treat all of them in the same way.⁶⁵

Although they have different physicochemical properties, bioisosteric functional groups are ideally capable to produce the same biological effect. For example, the bioisosteres phenyl, thienyl and pyridyl usually have the same biological effect although they are different in size, shape, electronic distribution, polarity, lipophilicity, hydrogen bond

formation capacity and pKa. Therefore, bioisosteric replacement within a drug molecule should maintain the same activity but change the drug's physicochemical properties.

Bioisosterism is utilized in the design and development of drugs to introduce varied structural changes, that are expected to have varied properties, for example: improved potency, superior selectivity, enhanced lipophilicity/hydrophilicity balance, improved pharmacokinetic properties, reduced affinity for metabolizing enzymes, or improved therapeutic index.⁶⁵⁻⁶⁷ Therefore, replacing a phenyl ring with a pyridyl ring as the "A" ring in the clofazimine structure (Figure 8) is anticipated to maintain the similar activity, improve the physicochemical properties, and consequently reduce the side effects and improve the pharmacokinetic properties of clofazimine. The addition of more hydrophilic substituents, along with the scaffold hopping, is anticipated to further increase the hydrophilicity and improve the pharmacokinetic properties. In this project, the focus was on systematic modification of R₁ and R₂ by introducing various substituents to the new scaffold (Figure 8).

Modifications to R₁ were based on substitution with isopropyl or hydrogen (Figure 9). The isopropyl group is the more lipophilic group that is found in clofazimine. The isopropyl effect on activity and physicochemical properties was tested by comparing compounds with the isopropyl group with their corresponding compounds that have a hydrogen as R₁.

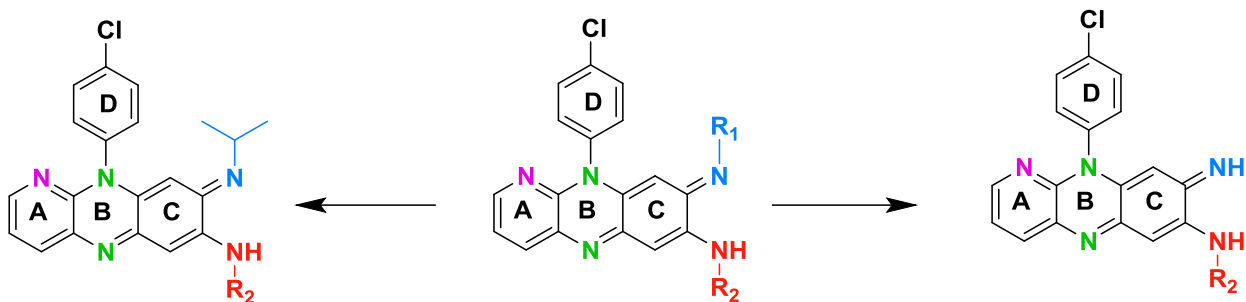


Figure 9. R₁ substitution with and isopropyl or a hydrogen.

Substitutions to R₂ were 4-chlorophenyl, 3-pyridyl, or 2-hydroxy-3-pyridyl (Figure 10). 4-chlorophenyl is the most lipophilic group and is found in clofazimine. The removal of the halogen and the addition of a nitrogen make 3-pyridyl a more hydrophilic substituent and the literature has also shown the 3-pyridyl to be the most active.⁶⁸ Moreover, the addition of a hydroxyl group to the 3-pyridyl makes 2-hydroxy-3-pyridyl the most hydrophilic substituent and is expected to improve the pharmacokinetic properties the most.

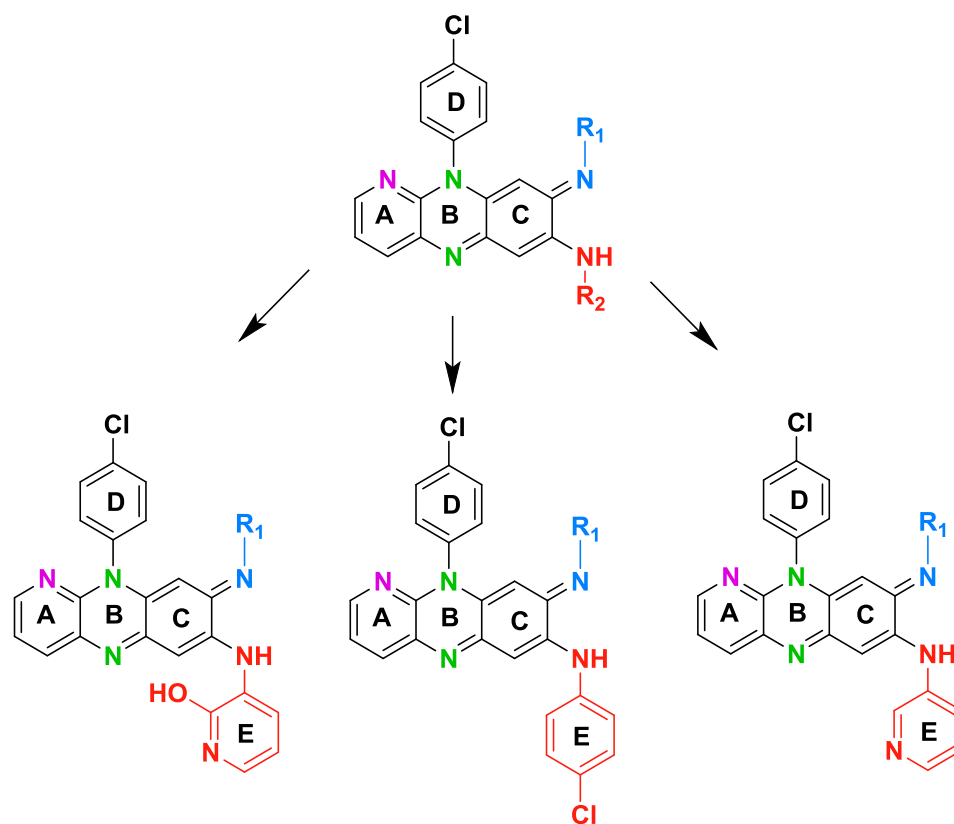


Figure 10. R₂ substitution with 4-chlorophenyl, 3-pyridyl, and 2-hydroxy-3-pyridyl.

A total of six analogs with anticipated lower lipophilicity were designed by the addition of hydrophilic atoms, such as nitrogen and oxygen, and the removal of lipophilic atoms, such as chlorine.

Table 1. R₁ and R₂ substituents based on the new scaffold for the synthesized analogs.

Compound	R ₁	R ₂
11	H	4-chlorophenyl

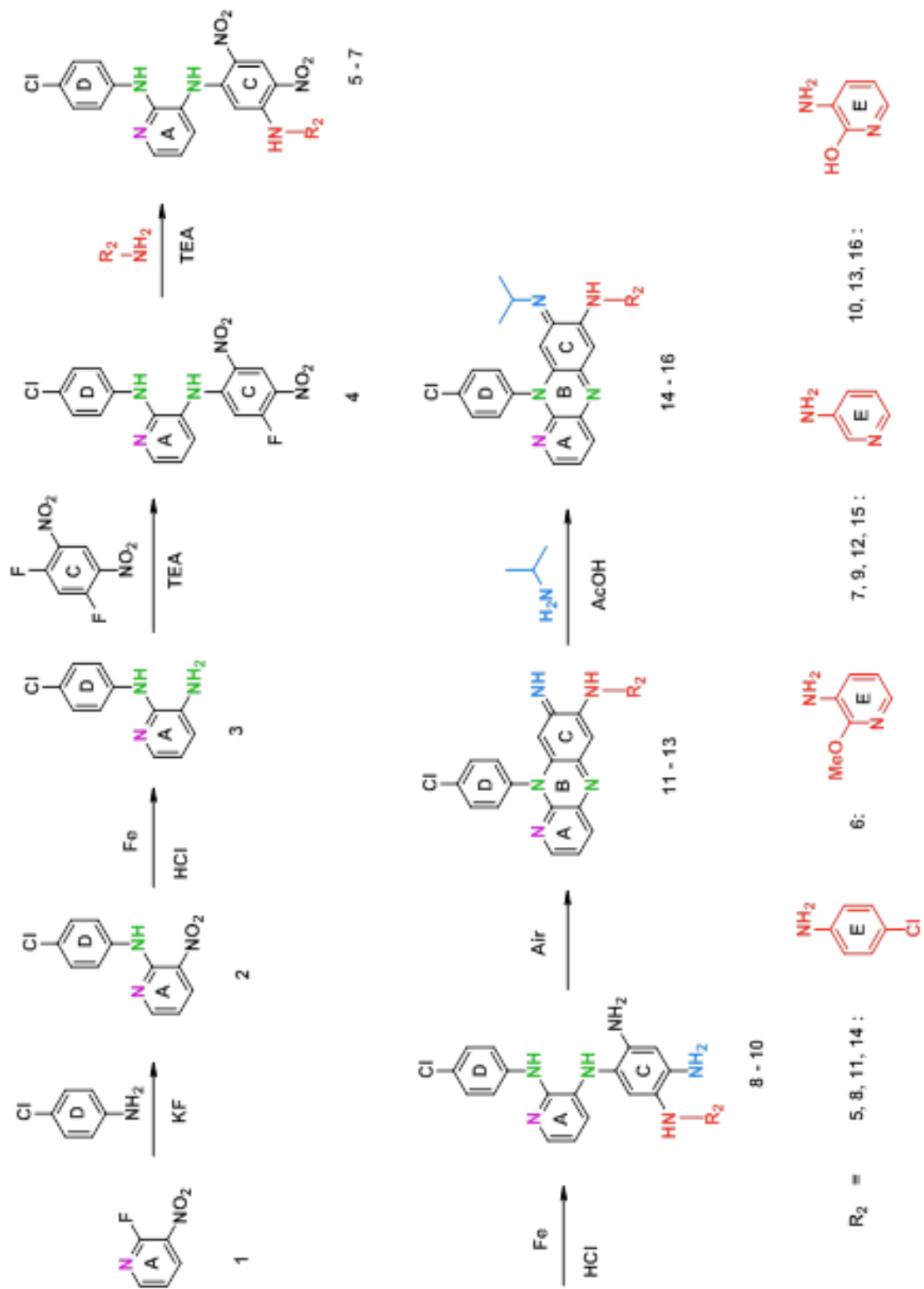
12	H	2-hydroxy-3-pyridyl
13	H	3-pyridyl
14	isopropyl	4-chlorophenyl
15	isopropyl	2-hydroxy-3-pyridyl
16	isopropyl	3-pyridyl

2.2 Synthesis and characterization of clofazimine analogs

The seven-step synthesis scheme (Scheme 1) was utilized for the synthesis of the clofazimine analogs.⁴⁴ Reactions were monitored by TLC for completeness and intermediates and products were characterized using mass spectrometry, ¹H and ¹³C NMR and UPLC with UV-vis detection.

The reactions used for the synthesis of clofazimine analogs will be discussed in the remaining of this chapter, please refer to Scheme 1 while reading through the following paragraphs.

Scheme 1. Synthesis of compounds 11-16



Reaction 1. Commercially available 2-fluoro-3-nitropyridine **1** was coupled to 4-chloroaniline by nucleophilic aromatic substitution reaction affording compound **2**. In this reaction, the nucleophilic aniline nitrogen attacks the partially positive C₂ carbon on the pyridine ring (Figure 11). The pi bond electrons are transferred to the C₃ carbon, forming a resonance-stabilized carbanion with the electron withdrawing nitro group. The presence of the *ortho*-electron withdrawing nitro group on the electrophile stabilizes the carbanion in the transition state and, therefore, makes it one of the high yielding reactions. Since the aromaticity of the phenyl ring is lost by forming the sp³ hybridized carbanion, this step is the rate-limiting step. Aromaticity of the benzene ring is then restored and fluorine leaves as F⁻. The amine nitrogen is now positively charged and bound to a highly acidic proton that is released in the media, converting the amine to a neutral secondary amine. This reaction is a neat reaction, which is a reaction that runs in the absence of solvent.

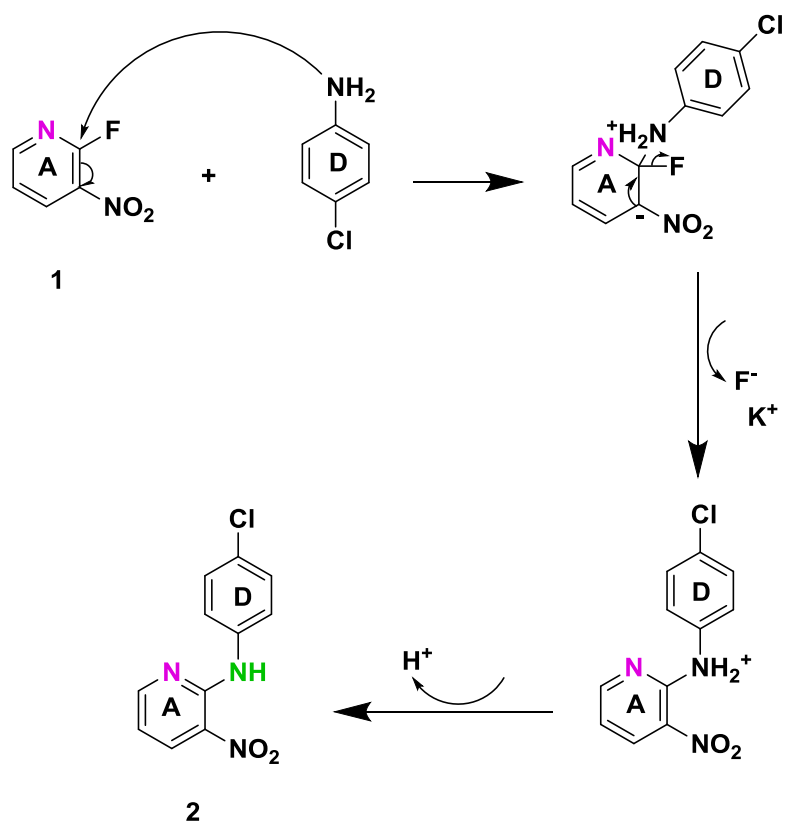


Figure 11. Nucleophilic aromatic substitution reaction mechanism for the coupling of ring A and ring D.

Reaction 2. The nitro group, found on compound 2, was reduced to an amine, in compound 3, using iron and hydrochloric acid. This reaction is one of the low yielding reactions and it needs further optimization. Although catalytic hydrogenation with H₂ and Pd/C efficiently reduces nitro groups to amines with little or no purification necessary, these conditions could potentially also substitute the halogens on ring D with hydrogen atoms. For that reason it was not chosen for initial reduction conditions and is not a venue to explore for optimization. However, HCl addition rate and solution temperature is one of the parameters that can be changed for optimization. For example, the addition of HCl all at once at room temperature resulted in many byproducts; however, cooling the

solution on an ice bath and adding the HCl slowly improved the yield and decreased the number of byproducts. Therefore, changing the starting material's temperature and HCl addition rate are parameters that can be explored for further optimization of this reaction to increase yield.

Reaction 3. Compound **3** was coupled to 1,5-difluoro-2,4-dinitro-benzene (DFDNB), in the presence of the weak base triethylamine (TEA), by nucleophilic aromatic substitution reaction to afford compound **4**. Figure 12 shows the mechanism of this reaction in which the primary amine in compound **3** is the nucleophile that attacks the DFDNB's fluorine. The presence of the *ortho*- and *para*-electron withdrawing nitro groups on the electrophile stabilizes the carbanion in the transition state and increases the DFDNB reactivity. Therefore, this reaction was performed under mild conditions and is a high yielding reaction.

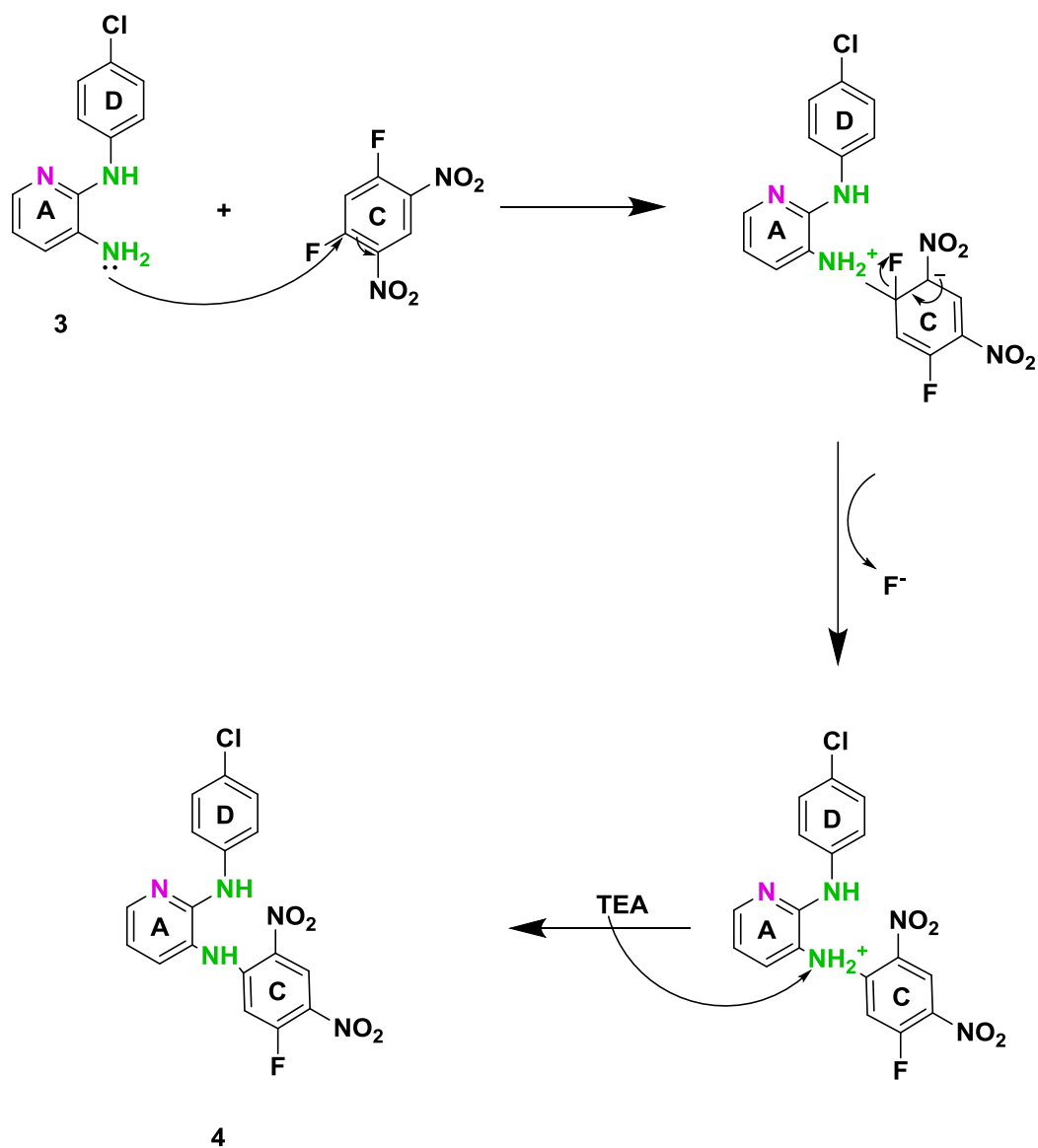


Figure 12. Nucleophilic aromatic substitution reaction mechanism for the addition of ring C.

Reaction 4. Ring E addition (R_2) is a point of diversity and product **4** was reacted with 4-chloroaniline, 3-amino-2-methoxypyridine, or 3-aminopyridine to afford intermediates **5–7**, respectively. This reaction is also a nucleophilic aromatic substitution reaction in

which the aniline nitrogen atoms in **R₂** (Figure 13) are the nucleophiles that attack the DFDNB's fluorine-carbon that did not react with compound **3**.

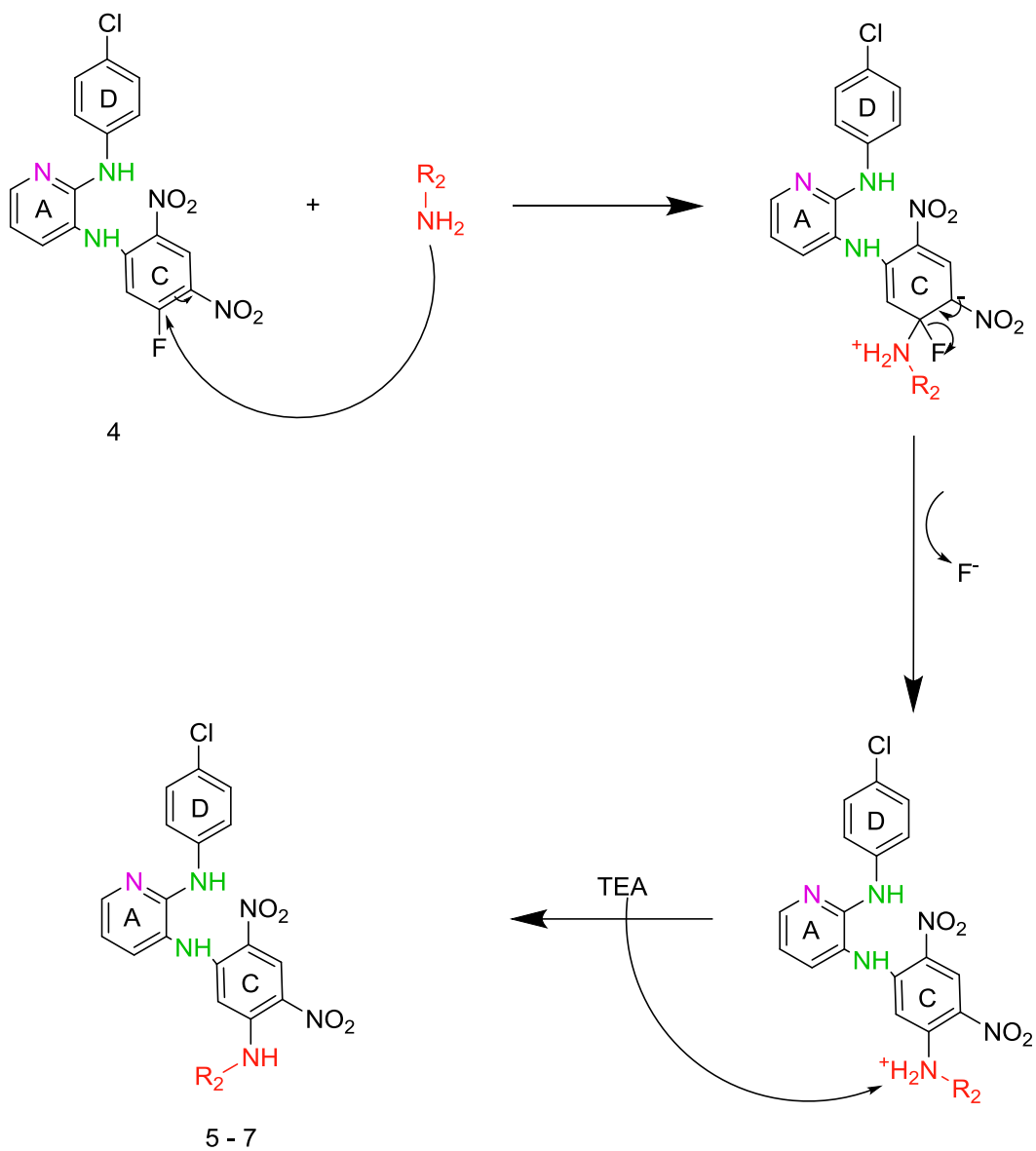


Figure 13. Nucleophilic aromatic substitution reaction mechanism for the addition of ring E.

Theoretically, different yields are expected based on the different nucleophilic strengths of the substituents when the same reaction conditions are used. The nitrogen on 4-chloroaniline has the lowest nucleophilic strength, since the presence of the electron withdrawing halogen deactivates the phenyl ring requiring the lone pair of electrons on the nitrogen to donate into the ring. 3-Amino-2-methoxypyridine is the strongest nucleophile, since it has the electron donating methoxy group on the *ortho*-position to the amine pushing electrons towards the amine nitrogen and making it a stronger nucleophile. The 3-aminopyridine has no electron withdrawing or electron donating groups, therefore, it is stronger than 4-chloroaniline and weaker than the 3-amino-2-methoxypyridine. However, 3-amino-2-methoxypyridine had the lowest practical yields due to the steric hindrance caused by the methoxy group ortho to the amine.

DFDNB is a strong electrophile. However, the removal of the electron withdrawing fluorine atom and the addition of the electron donating A and D rings make the electrophile more electron rich and therefore, less susceptible to nucleophilic attack. Therefore, this reaction required heating for overnight, while the previous one was stirred at room temperature for six hours.

In order to install a phenolic hydroxyl group into the E ring, protecting group chemistry was required. The methoxy group on the 3-amino-2-methoxypyridine is a protecting group. The final products **13** and **15** only contain the 2-hydroxypyridine-3-amine. The 2-hydroxypyridine-3-amine has two different nucleophiles, one is the nitrogen in the amine and the other is the oxygen in the alcohol. Both nucleophiles have the ability to displace the fluorine and bind to the C ring. In order to prevent a potential byproduct, the alcohol

was protected by the addition of the methoxy group. After the reaction was complete, the oxygen was subsequently dealkylated in the next reduction step.

Reaction 5. The nitro groups in products **5–7** were reduced to amine groups, and the methoxy group in product **6** was dealkylated using iron and hydrochloric acid. The reaction conditions were similar to the ones used for compound **2** reduction, except the reagents quantities were doubled because there were two different nitro groups to reduce. This reaction is also low yielding, has a complicated purification process, and needs further optimization.

Reaction 6. Compounds **8–10** spontaneously cyclize to the final products **11–13**, while they are in solutions exposed to air. The spontaneous cyclization was very fast, where compounds **8-10** could not be detected using MS and NMR after the reduction. MS and NMR data after the reduction corresponded to the final products **11-13**. The driving force of this reaction is the stability enhancement by forming a six-membered aromatic ring with the extended resonance throughout five different rings.

Regarding the spontaneous cyclization reaction (Figure 14) which forms the B ring, the resonance structure formed from the lone pair of electrons on the black amino group donating into the C ring results in a positively charged imine and an *ortho*-carbanion (Intermediate a). The positively charged black imino group is highly electron-withdrawing, making the adjacent carbon strongly partially positive and vulnerable to the attack of the green amino group between rings A and D. The green amino group becomes positively charged with a highly acidic proton after the bond formation with ring C (Intermediate b). Forming a bond with the green amino group breaks the newly formed

double bond with the black amine, making the black amine neutral (Intermediate b). The negative charge on the ring resonates back to form an aromatic ring and break the bond with the black amino group, which attacks the acidic hydrogen on the positive green amino group through a concerted intramolecular reaction (Intermediate c) and leaves as ammonia. The formed six-membered ring B is not aromatic and has a high energy state. However, O₂ in the air, after spontaneous hemolytic cleavage of its pi bond, attacks the remaining hydrogen through a radical mechanism on the green nitrogen and the bonded electrons separate forming a nitrogen radical (Intermediate d). The formed HO₂ radical subsequently attacks the hydrogen on the blue nitrogen forming another radical which terminate with each other to the fully aromatic three-membered core ring (Compounds **11-13**). The resulting H₂O₂ can undergo further reduction to 2H₂O by reaction with another radical.

The spontaneous cyclization is an oxidative cyclization reaction. Although the compounds did not gain oxygen atoms during the cyclization, oxidation reactions, by definition, require the loss of electrons, which happens in this reaction. The cyclized product has a lower number of electrons compared to the un-cyclized product and, therefore, it is considered an oxidized product.

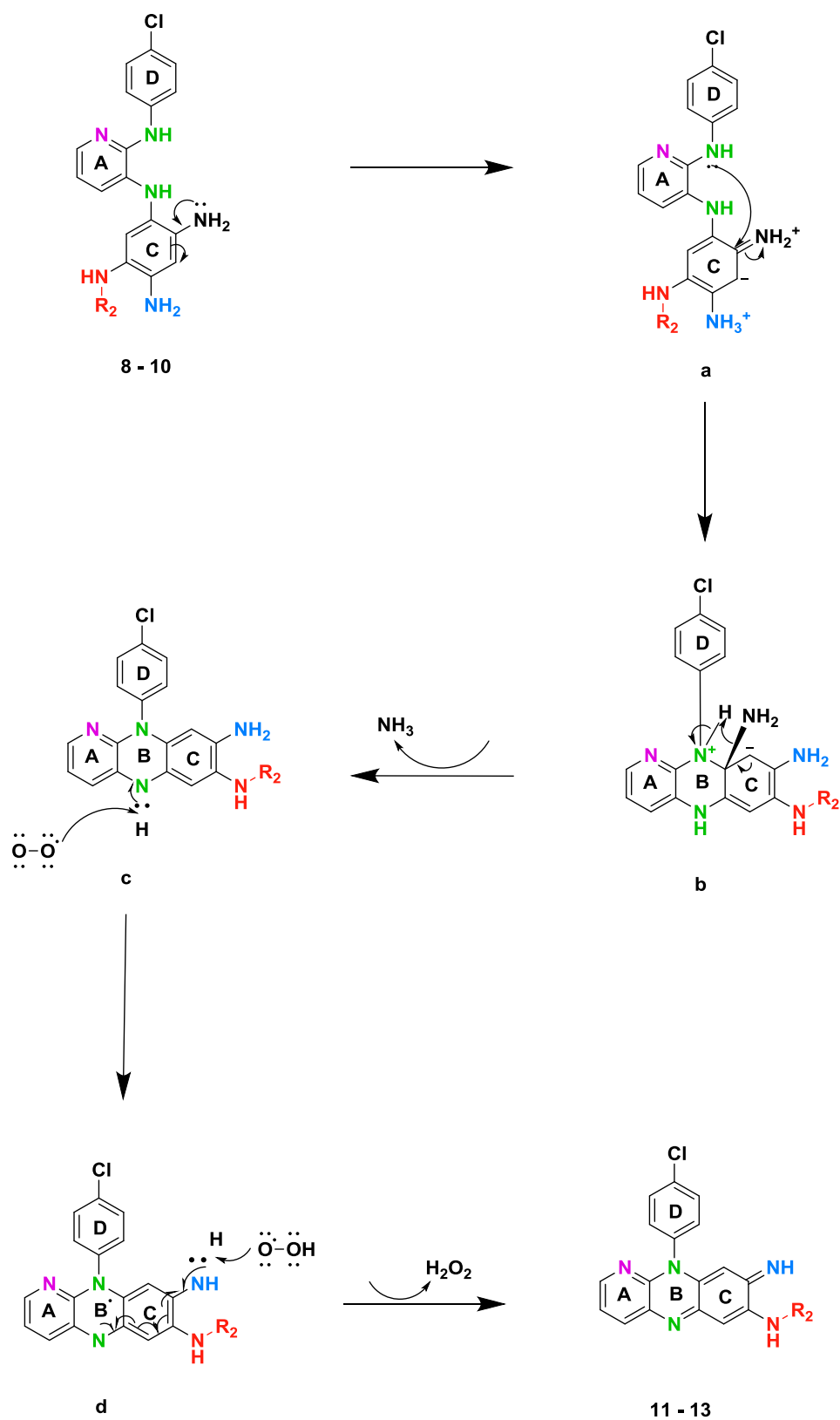


Figure 14. The mechanism for the spontaneous cyclization reaction.

Reaction 7. The imine in the final products **11-13** was substituted by an isopropyl group in the presence of glacial acetic acid to afford the final products **14-16**. In this reaction, the basic imine protonates in acidic conditions, making the adjacent carbon electrophilic (Figure 15). The isopropyl amine attacks the electrophilic carbon and the positively charged imine takes back the electrons in the double bond. The carbon is now bound to both the unsubstituted neutral amine and the positively charged isopropylamine. The positively charged isopropylamine gives one of its hydrogen atoms to the acetate conjugate base and is converted to a neutral aminal. Because the glacial acetic acid is reformed, the media is acidic enough to convert the unsubstituted neutral amine to a positively charged amine. The carbon is now bound to both the positively charged unsubstituted amine and the neutral isopropyl amine. The positively charged unsubstituted amine takes the sigma bond electrons and leaves as ammonia. The neutral isopropylamine forms a double bond with the carbon to become positively charged, and subsequently donates the remaining hydrogen atom to the acetate conjugate base. The reaction mechanism shows that the glacial acetic acid is a catalytic reagent reproduced throughout the reaction.

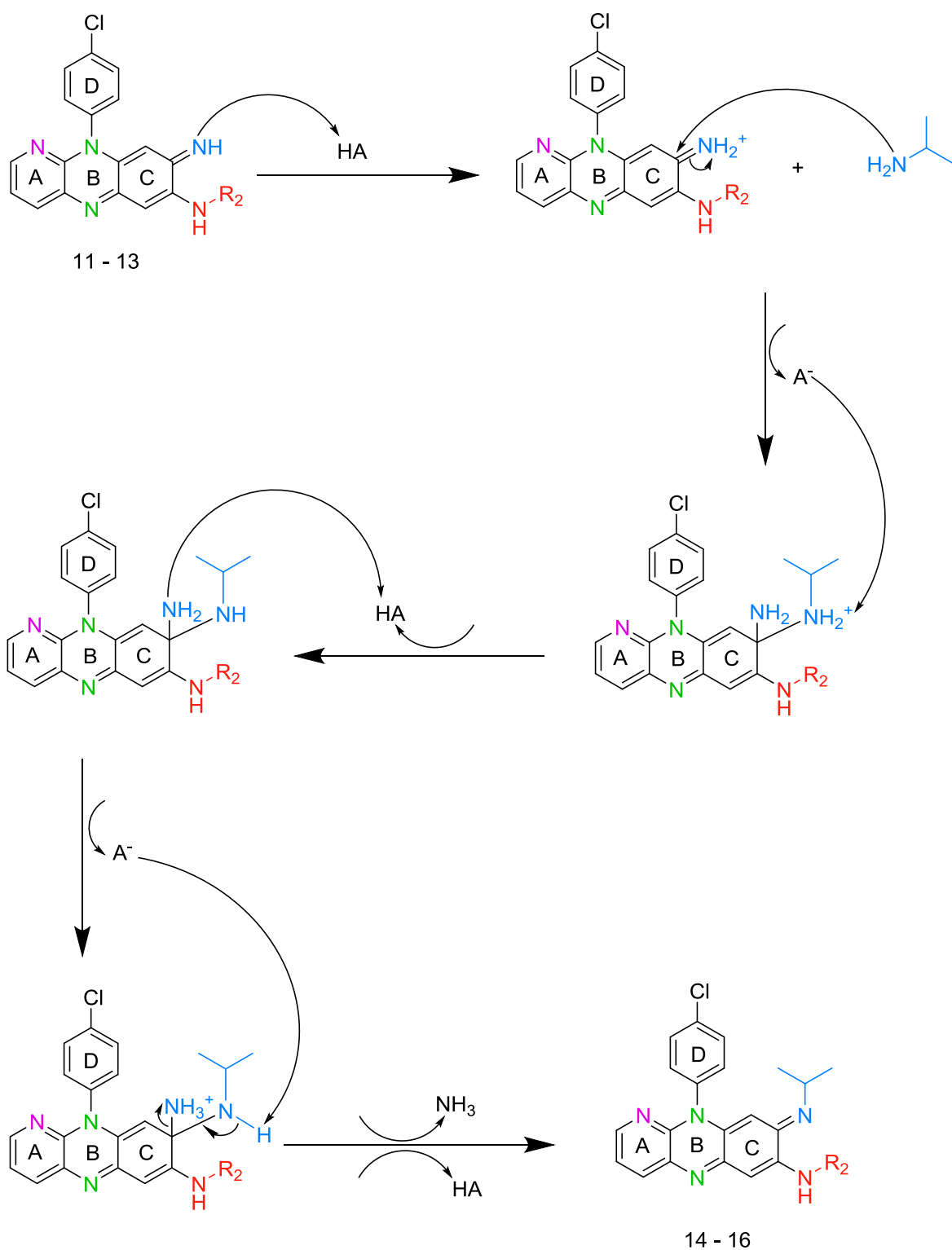
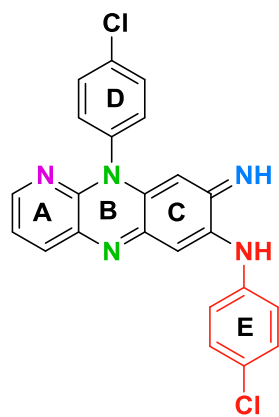


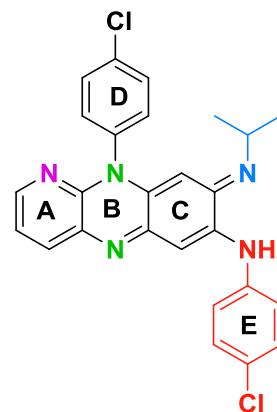
Figure 15. The mechanism for isopropyl amine addition.

2.3 Conclusion

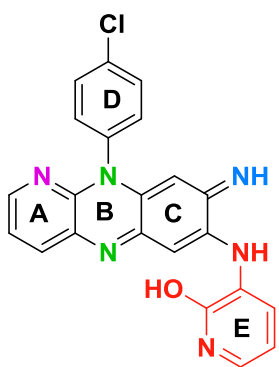
A seven-step reaction synthesis scheme was utilized to produce six different final products **11–16** (Figure 16). The yields were greater than 50% for all of the products, except for products **3** and **11**, which had a 50% yield, and products **12**, **13** and **15**, which had less than 50% yields. The primary low yielding reaction was the reduction reaction with a problematic purification and, therefore, it requires additional optimization. All of the final products were dark-colored, ranging from dark red to black with ultimate reaction yield range of 0.6 – 9.2%.



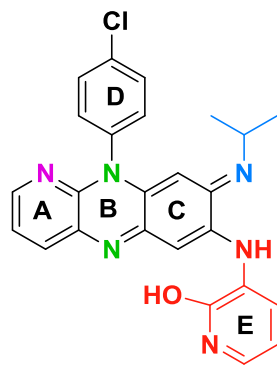
11



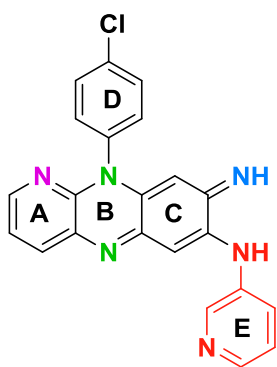
14



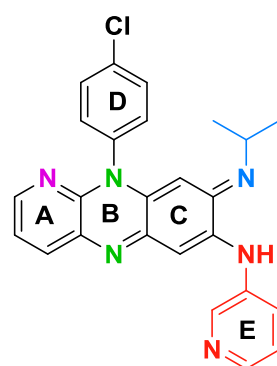
12



15



13



16

Figure 16. Final products 11 - 16

2.4 Experimental

2.4.1 Materials and instrumentation

All glassware was dried in a 150°C oven overnight. All chemicals, solvents, and glassware were purchased from either Fisher Scientific (Pittsburg, Pennsylvania) or Sigma Aldrich (St. Louis, Missouri). TLC plates, silica gel columns (100, 50, 25, and 10g), and C18 columns (30g) were purchased from Biotage[®] (Charlotte, North Carolina). The chemical reactions were tracked using fluorescent silica gel-coated TLC plates and the separated components were visualized using UV light (254 nm) or I₂. Compounds were purified using flash-column chromatography on a Biotage Isolera[™] with either silica gel or C18 silica. Mass spectra were acquired on an Agilent 1200 / AB Sciex[®] API 3200 QTrap LC/MS/MS, using electrospray ionization and a single quadrupole analyzer. All ¹H and ¹³C NMR spectra were obtained on an Ascend[™] 400 MHz Bruker spectrometer, and chemical shifts were reported relative to TMS. Waters Acquity Ultra Performance LC[™] was used for purity determination. An Acquity UPLC[®] BEH C18 column (1.7 μm) 2.1 X 100 mm column, flow rate of 0.45 mL/min, and a gradient of [solvent A (90 : 10 water : Acetonitrile with 0.1% formic acid) and solvent B (10 : 90 water : acetonitrile with 0.1% formic acid): 0–0.25 min 90% A; 0.25–3.0 min 90–0% A (linear gradient); 3.0–4.0 min 0% A; 4.0–4.75 min 0–100% A (linear gradient); 4.75–5.0 min 100% A] were used. UV absorbance (monitored at 254 nm) was used for detection of analytes. All compounds were found to have >95% purity [except compound **16**, which was found to have 94.03% purity].

2.4.2 Compound synthesis

2.4.2.1 Procedure for synthesis of *N*-(4-chlorophenyl)-3-nitropyridin-2-amine (2). 2-fluoro-3-nitropyridine (500 mg, 3.51 mmol), 4-chloroaniline (538 mg, 4.22 mmol) and anhydrous potassium fluoride (204 mg, 3.51 mmol) were stirred at 160 °C for overnight in a pressurized tube. After the mixture cooled, the reaction mixture was partitioned between water and ethyl acetate. The water layer was extracted with ethyl acetate twice, and the combined ethyl acetate layers were dried over anhydrous sodium sulfate. The solvent was evaporated under reduced pressure to give 555 mg of **2** as a red solid (65% yield). ¹H NMR (400 MHz, CDCl₃) δ: 8.55 (d, *J* = 8 Hz, 1H), 8.49 (d, *J* = 4 Hz, 1H), 7.62 (d, *J* = 4 Hz, 2H), 7.36 (d, *J* = 4 Hz, 2H), 6.86 - 6.88 (m, 1H). ESI/MS: *m/z* [M + H]⁺ calculated for C₁₁H₉ClN₃O₂: 250.7, found: 250.1.

2.4.2.2 Procedure for synthesis of *N*²-(4-chlorophenyl)pyridine-2,3-diamine (3). Compound **2** (1170 mg, 4.699 mmol) and iron powder (910 mg, 16.3 mmol) were sequentially added to ethanol (26 mL) and cooled on an ice bath for 30 minutes. Concentrated HCl (6 mL) was added to the reaction mixture portion wise over 15 minutes. The reaction was refluxed for 3.5 h at 90 °C. Upon cooling, the reaction mixture was diluted with water and neutralized to pH 8 by slow solid K₂CO₃ addition. The neutralized aqueous phase was extracted 3 times with ethyl acetate. The combined ethyl acetate layers were dried over anhydrous sodium sulfate and concentrated under reduced pressure. The crude mixture was purified by flash column chromatography on silica gel, using 0-30% ethyl acetate in hexane gradient, to give 505 mg of **3** as a tan solid (50% yield). ¹H NMR (400 MHz, DMSO-*d*₆) δ: 7.86 (s, 1H), 7.67 (d, *J* = 8 Hz, 2H), 7.50 (d, *J* = 8 Hz, 1H), 7.25 (d, *J* = 8 Hz, 2H), 6.91 (d, *J* = 8, 1H), 6.62 - 6.65 (m, 1H), 5.07 (s, 2H). ESI/MS: *m/z* [M + H]⁺ calculated for C₁₁H₁₁ClN₃: 220.7, found: 220.7.

2.4.2.3 Procedure for synthesis of N^2 -(4-chlorophenyl)- N^3 -(5-fluoro-2,4-dinitrophenyl)pyridine-2,3-diamine (4). Compound **3** (500 mg, 2.28 mmol), DFDNB (465 mg, 2.28 mmol) and TEA (231 mg, 2.28 mmol) were stirred in ethanol (35 mL) for 6 h at room temperature. The precipitated product was filtered and washed with ethanol to give 698 mg of **4** as an orange solid (76% yield). ^1H NMR (400 MHz, $\text{DMSO-}d_6$) δ : 9.98 (s, 1H), 8.95 (d, $J = 8$ Hz, 1H), 8.48 (s, 1H), 8.22 (d, $J = 4$ Hz, 1H), 7.67 (d, $J = 8$ Hz, 2H), 7.29 (d, $J = 4$ Hz, 2H), 6.94 - 6.96 (m, 1H), 6.46 (d, $J = 12$ Hz, 1H), 4.34 - 4.38 (m, 1H). ESI/MS: m/z $[\text{M} + \text{H}]^+$ calculated for $\text{C}_{17}\text{H}_{12}\text{ClFN}_5\text{O}_4$: 404.6, found: 404.5.

2.4.2.4 General procedure for synthesis of N^2 -(4-chlorophenyl)- N^3 -[5-(arylamino)-2,4-dinitrophenyl]pyridine-2,3-diamines (5-7). Compound **4** (690 mg, 1.7 mmol) and TEA (188 mg, 1.7 mmol) were dissolved in anhydrous THF (7 mL). To that, 4-chloroaniline (1 eq), 2-methoxypyridine-3-amine (1 eq), or 3-aminopyridine (1 eq) was added and refluxed for 18 h at 80 °C. After cooling, the reaction mixture was concentrated under reduced pressure and purified by flash column chromatography, using a 0-40% ethyl acetate in hexane gradient. Orange solids were obtained.

2.4.2.4.1 N^2 -(4-chlorophenyl)- N^3 -[5-(4-chlorophenylamino)-2,4-dinitrophenyl]pyridine-2,3-diamine (**5**): 75% yield, ^1H NMR (400 MHz, $\text{DMSO-}d_6$) δ : 9.64 (s, 1H), 9.54 (s, 1H), 9.02 (s, 1H), 8.39 (s, 1H), 8.07 (d, $J = 4$ Hz, 1H), 7.64 (d, $J = 8$ Hz, 2H), 7.55 (d, $J = 8$ Hz, 1H), 7.30 (d, $J = 8$ Hz, 2H), 7.22 (d, $J = 8$ Hz, 2H), 7.08 (d, $J = 8$ Hz, 2H), 6.84 - 6.86 (m, 1H), 5.76 (s, 1H). ESI/MS: m/z $[\text{M} + \text{H}]^+$ calculated for $\text{C}_{23}\text{H}_{17}\text{Cl}_2\text{N}_6\text{O}_4$: 512.3, found: 512.0.

2.4.2.4.2 N^2 -(4-chlorophenyl)- N^3 -[5-(2-methoxy-3-pyridylamino)-2,4-dinitrophenyl]pyridine-2,3-diamine (**6**): 92% yield, ^1H NMR (400 MHz, CDCl_3) δ : 9.73 (s, 1H), 9.36 (s, 2H), 8.24 (d, $J = 8$ Hz, 1H), 7.98 (d, $J = 4$ Hz, 1H), 7.52 (d, $J = 8$ Hz, 2H), 7.45 (d, $J = 8$ Hz, 1H), 7.28 - 7.31 (m, 3H), 6.83 - 6.86 (m, 1H), 6.62 - 6.72 (m, 1H), 6.64 (s, 1H), 6.05 (s, 1H), 3.92 (s, 3H). ESI/MS: $[\text{M} + \text{H}]^+$ calculated for $\text{C}_{23}\text{H}_{19}\text{ClN}_7\text{O}_5$: 508.1, found: 507.8.

2.4.2.4.3 N^2 -(4-chlorophenyl)- N^3 -[5-(3-pyridylamino)-2,4-dinitrophenyl]pyridine-2,3-diamine (**7**): 65% yield, ^1H NMR (400 MHz, CDCl_3 : Methanol- d_4 8 : 2) δ : 9.33 (s, 1H), 8.37 - 8.40 (m, 2H), 8.12 - 8.14 (m, 1H), 7.43 - 7.46 (m, 3H), 7.39 (s, 1H), 7.21 - 7.27 (m, 3H), 6.81 - 6.84 (m, 1H), 5.95 (s, 1H). ESI/MS: m/z $[\text{M} + \text{H}]^+$ calculated for $\text{C}_{22}\text{H}_{17}\text{ClN}_7\text{O}_4$: 478.9, found: 478.5, m/z $[\text{M} + 2\text{H}]^{2+}$ calculated for $\text{C}_{22}\text{H}_{18}\text{ClN}_7\text{O}_4$: 239.9, found: 239.7.

2.4.2.5 General procedure for the synthesis of 10-(4-chlorophenyl)-8-imino- N -(aryl)-8,10-dihydropyrido[2,3- b]quinoxalin-7-amines (11-13**).** Compound **5**, **6** or **7** (0.83 mmol) and iron powder (322 mg, 5.75 mmol) were mixed with ethanol (5 mL). The mixture was cooled on an ice bath for 30 minutes, to that HCl (2 mL) was added portion wise over 5 minutes. The reaction mixture was refluxed for 3.5 h at 90 °C. After cooling, the reaction mixture was diluted with water and then neutralized to pH 8 by adding K_2CO_3 slowly. The aqueous phase was extracted 3 times with ethyl acetate. The combined ethyl acetate layers were dried over anhydrous sodium sulfate and concentrated under reduced pressure. The crude mixture was purified by column chromatography using one of four methods. Method A, 20-100% methanol in methylene chloride gradient on silica gel. Method B, 0-50% methanol in ethyl acetate gradient on silica gel, followed

by 5-95% acetonitrile in water with 1% formic acid gradient on reversed phase silica. Method C, 0-30% ethyl acetate in hexane gradient on silica gel, followed by 5-95% acetonitrile in water with 1% formic acid gradient on reversed phase silica. Brown solids were obtained.

2.4.2.5.1 10-(4-chlorophenyl)-8-imino-*N*-(4-chlorophenyl)-8,10-dihydropyrido[2,3-b]quinoxalin-7-amine (**11**): method C, 50% yield. ¹H NMR (400 MHz, DMSO-*d*₆) δ: 9.90 (s, 1H), 8.09 (d, *J* = 4 Hz, 1H), 7.92 (d, *J* = 8 Hz, 1H), 7.74 (d, *J* = 8 Hz, 2H), 7.49 (d, *J* = 8 Hz, 2H), 7.44 (d, *J* = 4 Hz, 4H), 7.18 - 7.21 (m, 1H), 6.68 (s, 1H), 5.42 (s, 1H). ¹³C NMR (400 MHz, DMSO-*d*₆) δ: 165.2, 155.6, 151.2, 148.0, 146.2, 141.7, 139.4, 139.2, 139.0, 135.0, 134.1, 133.5, 133.2, 127.0, 123.5, 103.7, 102.9. ESI/MS: *m/z* [M + H]⁺ calculated for C₂₃H₁₆Cl₂N₅: 432.1, found: 432.7.

2.4.2.5.2 10-(4-chlorophenyl)-8-imino-*N*-(2-hydroxy-3-pyridyl)-8,10-dihydropyrido[2,3-b]quinoxalin-7-amine (**12**): method B, 28% yield. ¹H NMR (400 MHz, CDCl₃ : Methanol-*d*₄ 10:1) δ: 8.90 (s, 1H), 8.34 (d, *J* = 4 Hz, 1H), 8.24 (d, *J* = 8 Hz, 1H), 7.61 (d, *J* = 8 Hz, 1H), 7.50 (d, *J* = 8 Hz, 3H), 7.25 (d, *J* = 8 Hz, 2H), 6.92 - 6.95 (m, 1H), 6.78 (s, 1H), 6.27 (s, 1H). ¹³C NMR (400 MHz, CDCl₃ : Methanol-*d*₄ 10:1) δ: 156.5, 153.9, 151.5, 148.6, 139.3, 138.1, 136.8, 128.9, 122.5, 121.6, 117.7, 115.6, 112.9, 95.7. ESI/MS: *m/z* [M + H]⁺ calculated for C₂₂H₁₆ClN₆O: 415.1, found: 414.8, *m/z* [M + 2H]²⁺ calculated for C₂₂H₁₇ClN₆O: 208.1, found: 207.8.

2.4.2.5.3 10-(4-chlorophenyl)-8-imino-*N*-(3-pyridyl)-8,10-dihydropyrido[2,3-b]quinoxalin-7-amine (**13**): method A, 37% yield. ¹H NMR (400 MHz, DMSO-*d*₆) δ: 9.89 (s, 1H), 8.83 (s, 1H), 8.61 (s, 1H), 8.32 (d, *J* = 4 Hz, 1H), 8.11 (d, *J* = 4 Hz, 1H),

7.93 (d, $J = 8$ Hz, 1H), 7.85 (d, $J = 8$ Hz, 1H), 7.77 (d, $J = 8$ Hz, 2H), 7.52 (d, $J = 8$ Hz, 2H) 7.42 - 7.46 (m, 1H), 7.20 - 7.23 (m, 1H), 6.63 (s, 1H), 5.48 (s, 1H). ^{13}C NMR (400 MHz, DMSO- d_6) δ : 160.3, 151.4, 146.9, 145.0, 144.4, 142.6, 138.3, 136.5, 135.5, 135.0, 134.1, 131.5, 131.0, 128.9, 124.4, 119.8, 99.3, 98.2. ESI/MS: m/z $[\text{M} + \text{H}]^+$ calculated for $\text{C}_{22}\text{H}_{16}\text{ClN}_6$: 399.1, found: 399.0, m/z $[\text{M} + 2\text{H}]^{2+}$ calculated for $\text{C}_{22}\text{H}_{17}\text{ClN}_6$: 200.4, found: 199.9.

2.4.2.6 General procedure for the synthesis of 10-(4-chlorophenyl)-*N*-(aryl)-8-(2-propylimino)-8,10-dihydropyrido[2,3-*b*]quinoxalin-7-amines (14-16). Compound **11**, **12** or **13** (0.20 mmol) was mixed with isopropylamine (272 mg, 4.6 mmol) and glacial acetic acid (1.4 mg, 0.024 mmol) in 1 mL dioxane. The mixture was stirred and heated in a pressurized tube for overnight at 115 °C. After cooling, the reaction mixture was concentrated under reduced pressure and the residue was purified by flash column chromatography on silica gel using one of three methods. Method A: 0-20% ethyl acetate in hexane gradient. Method B: 0-50% methanol in ethyl acetate. Method C: 50-100% methanol in ethyl acetate. Red-brown solids were obtained.

2.4.2.6.1 10-(4-chlorophenyl)-*N*-(4-chlorophenyl)-8-(2-propylimino)-8,10-dihydropyrido[2,3-*b*]quinoxalin-7-amine (**14**): method A, 93% yield. ^1H NMR (400 MHz, CDCl_3 : Methanol- d_4 10:1) δ : 8.11 (d, $J = 4$ Hz, 1H), 7.90 (d, $J = 8$ Hz, 1H), 7.68 (d, $J = 8$ Hz, 2H), 7.28 - 7.37 (m, 6H), 7.10 - 7.13 (m, 1H), 5.43 (s, 1H), 3.47 - 3.53 (m, 1H), 1.12 (d, $J = 8$ Hz, 6H). ^{13}C NMR (400 MHz, CDCl_3 : Methanol- d_4 10:1) δ : 152.3, 150.3, 146.6, 144.6, 142.9, 138.2, 136.1, 135.7, 135.4, 134.6, 131.1, 130.9, 130.4, 129.5, 129.0, 123.2, 119.3, 98.6, 91.3, 23.6. ESI/MS: m/z $[\text{M} + \text{H}]^+$ calculated for $\text{C}_{26}\text{H}_{22}\text{Cl}_2\text{N}_5$: 474.1, found: 474.6.

2.4.2.6.2 10-(4-chlorophenyl)-*N*-(2-hydroxy-3-pyridyl)-8-(2-propylimino)-8,10-dihydropyrido[2,3-*b*]quinoxalin-7-amine (**15**): method B, 10% yield. ¹H NMR (400 MHz, CDCl₃ : Methanol-*d*₄ 10:1) δ: 8.90 (d, *J* = 4 Hz, 1H), 8.35 (d, *J* = 8 Hz, 1H), 8.25 (d, *J* = 8 Hz, 1H), 7.61 (d, *J* = 4 Hz, 1H), 7.50 (d, *J* = 8 Hz, 3H), 7.25 (d, *J* = 8 Hz, 2H), 6.92 – 6.95 (m, 1H), 6.80 (s, 1H), 6.26 (s, 1H), 1.71 (d, *J* = 4, 6H), 1.32 – 1.38 (m, 1H). ¹³C NMR (400 MHz, CDCl₃ : Methanol-*d*₄ 10:1) δ: 153.9, 151.5, 148.7, 147.5, 146.9, 145.6, 139.3, 138.1, 136.8, 134.9, 128.9, 127.8, 122.5, 121.6, 117.6, 115.6, 95.7, 94.9, 85.7, 29.1, 28.1. ESI/MS: *m/z* [M + H]⁺ calculated for C₂₅H₂₂ClN₆O: 457.1, found: 253.8, *m/z* [M + 2H]²⁺ calculated for C₂₅H₂₃ClN₆O: 229.1, found: 227.6.

2.4.2.6.3 10-(4-chlorophenyl)-*N*-(3-pyridyl)-8-(2-propylimino)-8,10-dihydropyrido[2,3-*b*]quinoxalin-7-amine (**16**): method C, 67% yield. ¹H NMR (400 MHz, CDCl₃ : Methanol-*d*₄ 10:1) δ: 8.56 (s, 1H), 8.31 (d, *J* = 4 Hz, 1H), 8.13 (d, *J* = 8 Hz, 1H), 7.92 (d, *J* = 12 Hz, 1H), 7.83 (d, *J* = 8 Hz, 1H), 7.69 (d, *J* = 4 Hz, 2H), 7.37 – 7.40 (m, 1H), 7.31 (d, *J* = 12 Hz, 2H), 7.12 - 7.16 (m, 1H), 6.79 (s, 1H), 5.45 (s, 1H), 3.49 – 3.55 (m, 1H), 1.13 (d, *J* = 4 Hz, 6H). ¹³C NMR (400 MHz, CDCl₃ : Methanol-*d*₄ 10:1) δ: 152.1, 150.2, 147.0, 144.3, 144.2, 143.5, 142.9, 136.9, 136.2, 135.6, 135.5, 134.9, 131.2, 130.9, 130.3, 128.7, 124.2, 119.4, 99.2, 91.3, 23.6. ESI/MS: *m/z* [M + H]⁺ calculated for C₂₅H₂₂ClN₆: 441.9, found: 441.2, *m/z* [M + 2H]²⁺ calculated for C₂₅H₂₃ClN₆: 221.5, found: 221.2.

Chapter 3

Activity and physicochemical characterization of
synthesized clofazimine analogs

After compound synthesis, the maintained activity and the improved pharmacokinetic properties were confirmed. If the new scaffold (Figure 8) reduces antimycobacterial activity, the synthesized analogs are unsuitable candidates for TB treatment. Also, if the new compounds do not have improved physicochemical properties, they will not likely be able to improve clofazimine's side effect and toxicity profiles.

In vivo determination of the anti-TB activity and/or pharmacokinetic properties is not a viable option for early-stage analysis of novel clofazimine analogs. However, *in vitro* activity, predicted physicochemical properties, and *in vitro* measures of drug solubility and permeability are possible to characterize novel clofazimine analogs and guide future compound synthesis and *in vivo* studies.

3.1 The new scaffold is active against *M. tuberculosis*

In order to verify that the new scaffold maintains antitubercular activity, *in vitro* whole-cell screening of the compounds was used to determine the MIC against *M. tuberculosis*.

Table 2 summarizes the MIC values for clofazimine and the synthesized analogs.

Table 2. MIC of clofazimine and the synthesized analogs.

Compound	R ₁	R ₂	MIC (µg/mL)
Clofazimine	isopropyl	4-chlorophenyl	< 0.2
11	H	4-chlorophenyl	0.8
12	H	2-hydroxy-3-pyridyl	100
13	H	3-pyridyl	0.8

14	isopropyl	4-chlorophenyl	25
15	isopropyl	2-hydroxy-3-pyridyl	50
16	isopropyl	3-pyridyl	< 0.2

Modification of the scaffold by the addition of the hydrophilic nitrogen containing A ring maintains antitubercular activity. Compounds **11**, **13**, and **16** are highly potent, since the MIC is comparable to ethambutol's MIC,⁶⁹ one of the first line anti-TB agents. Therefore, they are considered promising leads for further investigation.

Changing the structure by substituting R₂ with a 3-pyridyl has the most positive impact on activity (Compounds **13** and **16**). However, substituting R₂ with 2-hydroxy-3-pyridyl (Compounds **12** and **15**) drastically decreases the activity and, therefore, the significant increase in hydrophilicity by the addition of hydroxyl groups is not favorable. Activity changes by substituting R₂ with 4-chlorophenyl depends on R₁ group. If R₁ is an isopropyl, the activity decreases (Compound **14**) and if it is a hydrogen, the activity is maintained (Compound **11**).

Changing the R₁ substituents does not have a significant impact on activity. When the R₂ substituent is the same, R₁ substitution with the isopropyl group tends to have a little higher activity than the substitution with the hydrogen. However, as mentioned earlier this is not the case when the R₂ substituent is 4-chlorophenyl.

3.2 Clofazimine analogs have lower Clog P values

The log transformed partition coefficient (log P) is an *in vitro* measure of a drug's ability to partition between organic and aqueous phases. The log P value can influence the pharmacokinetic properties of drugs. For example, large log P values indicate a drug has a high lipophilicity and lipid solubility. On the other hand, low log P values suggest a drug has higher hydrophilicity and water solubility. Clofazimine has a tremendously high calculated partition coefficient (Clog P) of 7.8. This value suggests that clofazimine is poorly distributed throughout the body but sequestered in lipophilic tissues and is supported by experimental evidence showing accumulation of clofazimine crystals in fatty tissues throughout the body. The high log P value contributes to clofazimine's poor pharmacokinetic properties and severe side effects. For novel clofazimine analogs to have improved pharmacokinetic properties compared to the parent clofazimine molecule, analog log P values must be lowered (i.e. the log P value has to be small enough for a drug to be solubilized in biological fluids, and large enough to allow the permeation across the biological membranes). Any lowering of clofazimine's log P value would potentially be beneficial with desirable log P values equal to or less than five.

The addition of a nitrogen to clofazimine's central core ring structure (Figure 8) was designed to create analogs with lower Clog P values (Table 3). Lower Clog P values are anticipated to improve the aqueous solubility and permeability of analogs and eventually lead to improved pharmacokinetic properties. Compounds with lower log P values are easier to be solubilized in the aqueous biological fluids, and ultimately permeate through the lipophilic membranes.

Table 3. Clog P values, calculated using Schrodinger QikProp software, for clofazimine and the synthesized analogs.

Compound	R₁	R₂	Clog P
clofazimine	isopropyl	4-chlorophenyl	7.8
11	H	4-chlorophenyl	5.8
12	H	2-hydroxy-3-pyridyl	4.2
13	H	3-pyridyl	4.4
14	isopropyl	4-chlorophenyl	7.2
15	isopropyl	2-hydroxy-3-pyridyl	5.6
16	isopropyl	3-pyridyl	5.7

The Clog P value of compound **14** is 0.6 units lower than clofazimine log P. Thus, the introduction of the nitrogen atom in the scaffold improves the Clog P value. The removal of the isopropyl group as R₁ substituent has a major impact on the Clog P value. The Clog P value decreases at least 1.3 units for compounds having hydrogen as the R₁ substituent, compounds **11**, **12** and **13**, as compared with compounds that have the isopropyl, compounds **14**, **15** and **16**, respectively.

For R₂ substituents, the comparison between compounds **11** versus **13** and compounds **14** versus **16** shows that the removal of the chlorine and the introduction of the nitrogen has the most significant impact on log P, decreasing Clog P values by at least 1.4 units. However, the introduction of the hydroxyl group does not significantly improve the Clog P, as shown in compounds **15** versus **16** and compounds **12** versus **13**.

3.3 Clofazimine and its analogs can be quantified using a validated method on UPLC

Clofazimine and the analogs should be reliably quantified in a well-established method in order to be able to determine their concentrations in the solubility and the permeability testing. After changing experimental parameters, a UPLC quantification method was developed and optimized. The absorbance of clofazimine and its analogs at 286 and 492 nm determined using a photo diode array (PDA) detector. Figure 17 shows the resulting chromatogram with clofazimine having a retention time of 1.55 minutes.

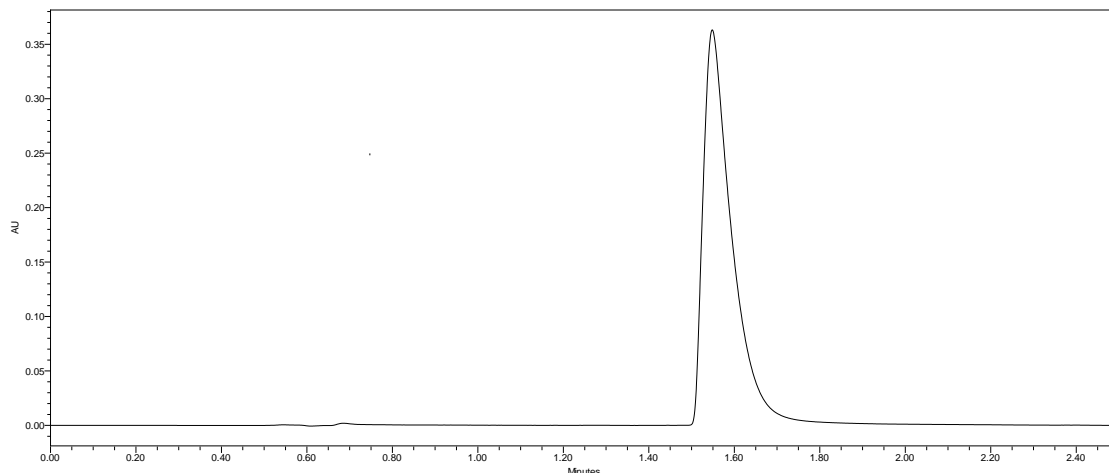


Figure 17. Absorbance vs. time plot of clofazimine at 286 nm.

Clofazimine has two different absorption maxima, 286 and 492 nm (Figure 18). Since 286 nm is the wavelength of maximum absorbance, it was used for the detection of low concentrations of clofazimine to improve method sensitivity. When multiple interfering components were present in the sample, 492 nm was used to selectively detect clofazimine because it is very rare to find a compound that absorbs at such a long wavelength. The UPLC method was validated according to the FDA guidelines.⁷⁰

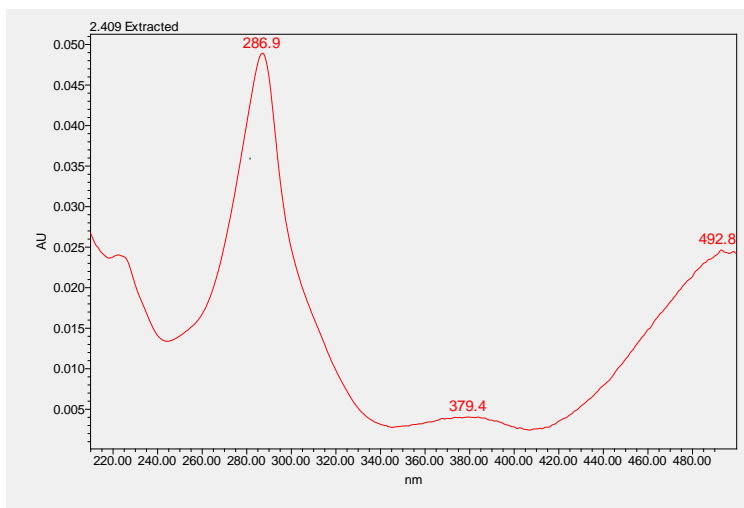


Figure 18. Clofazimine UV absorbance spectrum

3.3.1 Standard Curve

The standard curve is the relationship between the absorbance and concentration of samples. The area under the curve (AUC) of the chromatogram (Figure 17) was used to quantify UV absorbance. Thirty samples with a concentration range of (9.3×10^{-7} – 500 $\mu\text{g/mL}$) were prepared in mobile phase, without an internal standard, and injected using the method described above. For 286 nm, the limit of detection (LOD), which is clofazimine concentration that absorbs three times the blank absorbance, was 0.007 $\mu\text{g/mL}$, and the limit of quantification (LOQ), which is clofazimine concentration that

absorbs ten times the blank absorbance, was 0.03 $\mu\text{g/mL}$. For 492 nm, the LOD was 0.03 $\mu\text{g/mL}$ and the LOQ was 0.12 $\mu\text{g/mL}$. The detector was saturated above 62.5 $\mu\text{g/mL}$ at both wavelengths. Therefore, the standard curve was linear in the range of (0.03 – 62.5 $\mu\text{g/mL}$) for 286 nm (Figure 19) and (0.12 – 62.5 $\mu\text{g/mL}$) for 492 nm (Figure 20). The derived equations were used to calculate the concentration of unknown samples based on their AUC in the resulting chromatogram in the solubility and the permeability studies. The comparison between the two equations show that the intercept is larger for 286 nm, which supports the fact that 492 nm is more selective and it is less likely to find compounds at this wavelength.

The R^2 values were 0.9999 for both wavelengths. Thus, there is a linear direct relationship between the absorbance and the concentration. The linear direct relationship means that any given increase in the concentration will always produce a corresponding increase in the absorbance.

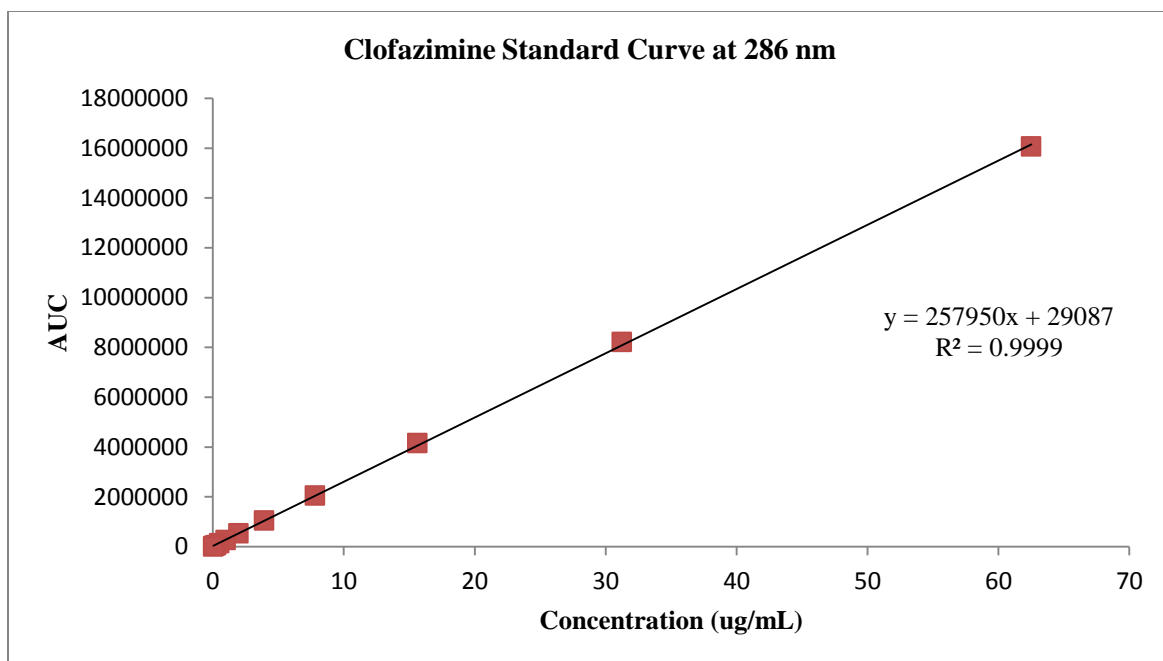


Figure 19. Clofazimine concentration vs. the area of the absorbance curve at 286 nm.

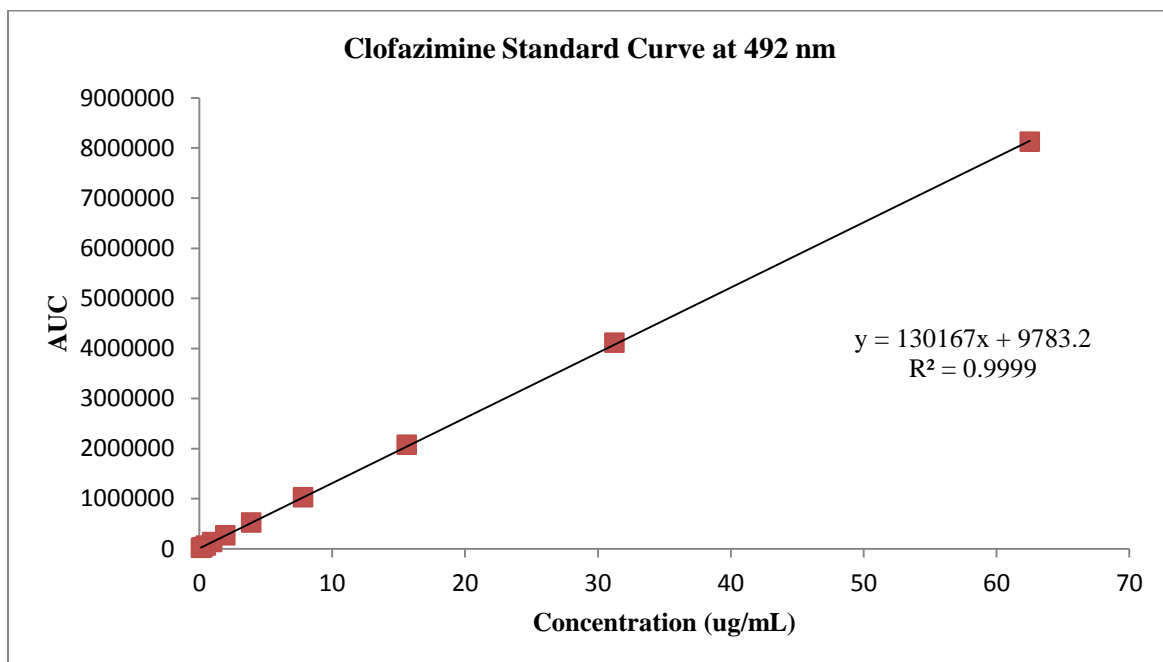


Figure 20. Clofazimine concentration vs. the area of the absorbance curve at 492 nm.

3.3.2 Accuracy

Accuracy describes how close the calculated concentration, obtained from the derived equation, to the true concentration, the actual amount of clofazimine dissolved in the sample. According to the FDA, the mean value of the calculated concentrations should be within 15% difference from the true concentration. Four different concentrations in the range of expected concentrations were tested. All of the measured concentrations at both 286 (Table 4) and 492 (Table 5) nm were within 6% difference from the true value, concluding that the UPLC method of quantification is accurate.

Table 4. Mean of the calculated values of four different concentrations and the percent of the true concentration at 286 nm.

Theoretical concentration (µg/mL)	Mean of calculated concentrations (µg/mL)*	Percent of the true concentration
0.1	0.10 ± 0.009	100.0
10	9.66 ± 0.063	96.6
20	19.79 ± 0.109	98.9
40	39.37 ± 0.242	98.4

* N = 5

Table 5. The mean of the calculated values of four different concentrations and their percent of the true concentration at 492 nm.

Theoretical concentration (µg/mL)	Mean of calculated concentrations (µg/mL)*	Percent of the true concentration
0.1	0.11 ± 0.003	106.1
10	9.66 ± 0.069	96.6
20	19.64 ± 0.111	98.2
40	39.12 ± 0.244	97.8

* N = 5

3.3.3 Precision

Precision describes how close the measured responses of multiple aliquots of the same homogenous analyte to each other when the same method is applied repeatedly. Precision is further divided into intra-day and inter-day precision. In intra-day precision, all the responses recorded in the same day. However, for the inter-day precision the responses are recorded in three different days. According to the FDA, the coefficient of variance (CV) at each concentration level should not exceed 15%. Four different concentrations in the range of expected experimental concentrations were tested, with the AUC being the response. The CV of all the intra-day and inter-day measured responses at both 286 (Table 6) and 492 (Table 7) nm were less than 5%, concluding that the UPLC method of quantification is precise.

Table 6. The mean and the CV of the AUC for both inter-day and intra-day precision at 286 nm.

Concentration ($\mu\text{g/mL}$)	Intra-day*		Inter-day**	
	Mean AUC ($\mu\text{V}\cdot\text{sec}$)	CV (%)	Mean AUC ($\mu\text{V}\cdot\text{sec}$)	CV (%)
0.1	2,566 \pm 229	0.89	26136 \pm 913	3.49
10	2,559,591 \pm 16,095	0.63	2,531,905 \pm 34,511	1.36
20	5,159,802 \pm 28,072	0.54	5,076,015 \pm 112,971	2.23
40	10,189,142 \pm 62,030	0.61	10,017,480 \pm 273,234	2.73

* N = 5

** N = 15

Table 7. The mean and the CV of the AUC for both inter-day and intra-day precision at 492 nm.

Concentration	Intra-day*	Inter-day**

($\mu\text{g/mL}$)	Mean AUC ($\mu\text{V}\cdot\text{sec}$)	CV (%)	Mean AUC ($\mu\text{V}\cdot\text{sec}$)	CV (%)
0.1	12,761 \pm 392	3.08	13,301 \pm 632	4.75
10	127,6547 \pm 9,083	0.71	1,265,134 \pm 15,767	1.25
20	2,576,871 \pm 14,342	0.56	2,537,763 \pm 54,189	2.14
40	5,103,690 \pm 31,632	0.62	5,017,595 \pm 136,026	2.71

* N = 5

** N = 15

3.4 The synthesized compounds have improved solubility

The solubility of clofazimine in different solvents (Figure 21) was tested using the thermodynamic solubility technique. Clofazimine solubility in water is 2.48 $\mu\text{g/mL}$ and according to the United States Pharmacopoeia (USP) it is considered a practically water

insoluble drug. However, clofazimine was highly soluble in organic solvents, having the highest solubility in methylene chloride.

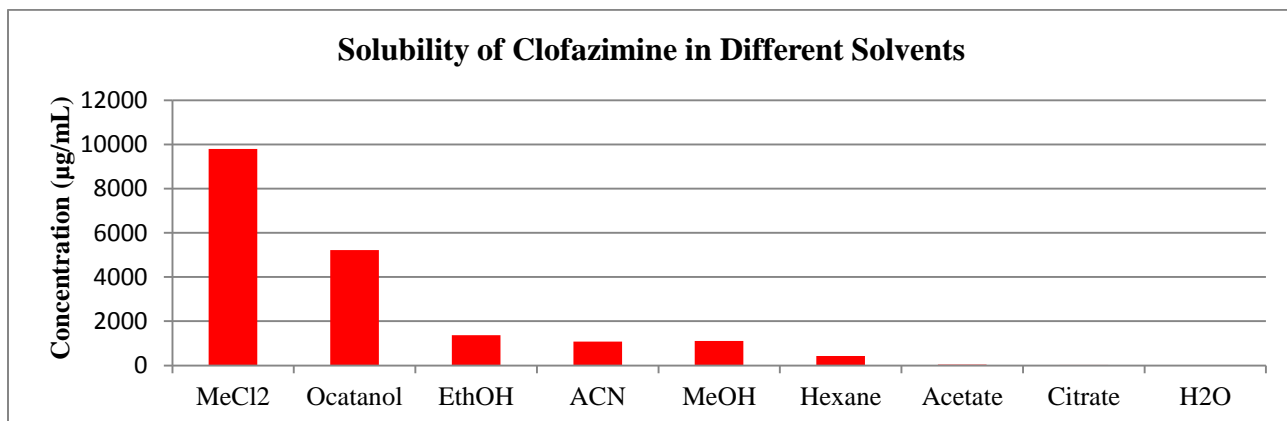


Figure 21. Thermodynamic solubility of clofazimine in different solvents (N = 1)

Clofazimine's poor aqueous solubility is one of the consequences of its high log P value. Compounds with low log P values tend to have improved aqueous solubility. If the compound is more water soluble, it has a lower affinity to lipids and subsequently a lower tendency for accumulation in lipids, such as the skin and cell membranes. Therefore, the improved solubility is one of the proxy measures for the improved pharmacokinetic properties.

The kinetic solubility was determined for the synthesized compounds. Kinetic solubility is an early stage screen that needs only small amounts of compounds, and highly predictive for thermodynamic solubility.⁷¹ Table 8 summarizes the solubility data for clofazimine and the synthesized analogs in simulated lung fluid (SLF).

Table 8. Kinetic solubility of clofazimine and six different analogs in SLF.

Compound	R ₁	R ₂	Solubility (µg/mL)*
clofazimine	isopropyl	4-chlorophenyl	1.47
11	H	4-chlorophenyl	1.48
12	H	2-hydroxy-3-pyridyl	15.28
13	H	3-pyridyl	3.66
14	isopropyl	4-chlorophenyl	1.29
15	isopropyl	2-hydroxy-3-pyridyl	11.96
16	isopropyl	3-pyridyl	2.90

*N = 3

All of the synthesized compounds have improved solubility. The solubility of compounds **11** and **14** are very close to clofazimine solubility. Therefore, solely changing the central core of clofazimine, by adding the nitrogen containing A ring, does not affect the solubility. Also, the removal of the isopropyl group, as R₁, does not have a significant impact on solubility as shown by the solubility of compounds **11**, **12** and **13** compared to the solubility of compounds **14**, **15** and **16**, respectively.

However, the addition of hydrogen bond forming atoms on R₂ drastically improves solubility. For example, compounds **13** and **16** have 3-pyridyl, which has a nitrogen atom as a hydrogen bond acceptor, and their solubility became two times larger than clofazimine solubility. Also, substituting R₂ with the 2-hydroxy-3-pyridyl, which has a

nitrogen and an oxygen as hydrogen bond forming atoms, increases the solubility in compounds **12** and **15** to become up to 10 times larger than clofazimine solubility.

3.5 The synthesized analogs are more permeable than clofazimine

Clofazimine's poor permeability is also one of the consequences of its high log P. Compounds with lower log P values tend to have improved permeability, which translates to the lower tendency for lipid accumulation. Thus, the drug permeability through an artificial membrane provides an indication of *in vivo* drug distribution.

Parallel artificial membrane permeation assay (PAMPA) is widely used as an *in vitro* model with a high correlation with the *in vivo* permeability studies ($R^2 = 0.87$).⁷² This model uses a 96-well filter-based donor plate that is placed upon a 96-well acceptor plate. The compound of interest is allowed to passively permeate through the membrane from the donor to the acceptor plate (Figure 22). Drugs with high permeability through the membrane will have high acceptor concentrations.

The polyvinylidene fluoride (PVDF) filter was converted to an artificial membrane by the application of 1% w/v lecithin in dodecane solution. Lecithin is a mixture of amphiphilic molecules that have hydrophilic heads and lipophilic tails. Mimicking membrane phospholipids in mammals, the amphiphilic molecules in lecithin are arranged uniformly over the filter support forming a membrane-like phospholipid bilayer. For this assay, the manufacturer's suggested protocol was used.⁷³

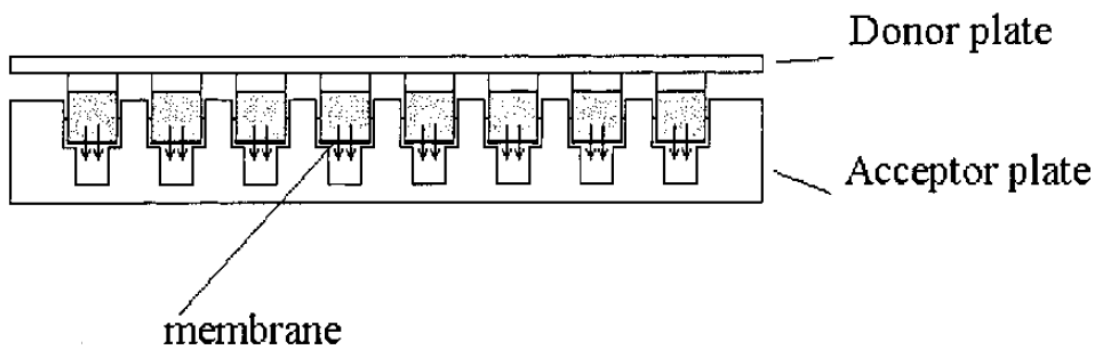


Figure 22. Drug passive diffusion from donor to acceptor plates through an artificial membrane in PAMPA setup.⁷³

Table 9 summarizes the permeability data for clofazimine and its analogs. Equation 1 was used for the calculation of the apparent permeability (P_e)⁷⁴:

$$P_e = \left[\frac{V_D \times V_A}{(V_D + V_A) \times Area \times Time} \right] \times \left\{ -\ln \left[1 - \frac{C_A(t)}{C_{eq.}} \right] \right\}$$

Equation 1. Apparent permeability (P_e) calculation.

where (V_D) is the volume of the donor compartment, (V_A) is the volume of the acceptor compartment, (**Area**) is the area of the membrane times the porosity, (**Time**) is the incubation time, ($C_A(t)$) is the concentration of the acceptor compartment after incubation, and ($C_{eq.}$) is the equilibrium concentration. The fraction of the compound that is retained in the membrane (R) is calculated using Equation 2⁷⁵:

$$R = 1 - \left[\frac{C_D(t)}{C_D(0)} \right] - \left\{ \left(\frac{V_A}{V_D} \right) \times \left[\frac{C_A(t)}{C_D(0)} \right] \right\}$$

Equation 2. Compound retention in the membrane (R) calculation.

where ($C_D(0)$) and ($C_D(t)$) are the concentrations in the donor compartment before and after incubation, respectively. Low R values suggest a lower tendency for accumulation in the biological membranes and consequently a lower accumulation in fatty tissues.

Table 9. Acceptor, donor and drug equilibrium concentrations of clofazimine and its analogs that have been used for the calculation of the apparent permeability (P_e) and the fraction retained in the membrane (R).

Compound	Acceptor concentration* ($\mu\text{g/mL}$)	Donor Concentration* ($\mu\text{g/mL}$)	Drug equilibrium concentration ($\mu\text{g/mL}$)	$P_e \times 10^{-3}$ (cm/s)	R
clofazimine	undetectable	undetectable	0.435	< 0.88**	> 0.997**
11	0.146	0.332	3.676	1.26	0.950
12	undetectable	4.446	4.063	< 45.45**	> 0.144**
13	3.127	2.506	3.560	65.27	0.299
14	0.027	0.213	0.249	3.55	0.979
15	1.359	1.580	2.488	24.48	0.656
16	1.105	0.923	3.244	12.91	0.749

* N = 4

** P_e and R were calculated based on the LOQ

Clofazimine was not able to permeate through the membrane due to its high lipophilicity and, therefore, was not detected in the acceptor compartment. All of the analogs have improved permeability compared to clofazimine. Thus, the addition of the nitrogen atom

to the central core for all clofazimine analogs (Figure 8) improves the *in vitro* permeability and suggests the analogs are able to move across the membrane.

Compounds **11** and **14** have a modest improvement in permeability, suggesting that the addition of the nitrogen atom to the central core and/or the removal of the isopropyl group as R₁ substituent do not have a significant impact on permeability. This also suggests that the lipophilic 4-chlorophenyl is the biggest barrier against permeability improvement.

Compound **12** has a very low absorptivity with a high LOQ and it was not able to be detected in the acceptor compartment. The LOQ was used for calculations and suggested a potential permeability improvement and a P_e value that can be as high as 45.45x10⁻³ cm/s.

However, compounds **13**, **15** and **16** have at least 14-fold improved P_e values. Thus, 3-pyridyl or 2-hydroxy-3-pyridyl R₂ substitution is able to improve permeability. Since isopropyl is lipophilic, compounds with the isopropyl substituents, compounds **15** and **16**, had less improvement than compound **13** with the hydrogen.

Almost all of the clofazimine was retained in the membrane, with R-values approaching 1. R-values were decreased for all of the analogs compared to clofazimine suggesting the addition of the nitrogen atom to the central core decreased the retention propensity in the lipophilic membranes. Compound **13** has the lowest detected R value of 0.299.

3.6 Conclusion

An optimized and validated method of quantification on UPLC was used for the quantification of clofazimine and its analogs. The new scaffold is active against TB and all of the synthesized analogs have improved log P, solubility and permeability. Three of the synthesized analogs, compounds **11**, **13** and **16**, are highly potent against *M. tuberculosis* with MIC values ≤ 0.8 $\mu\text{g/mL}$. However, all three compounds have poor solubility, with solubility values lower than 4 $\mu\text{g/mL}$. Two of the compounds, compounds **13** and **16**, have good permeability with P_e values of at least 14-fold better than clofazimine, and only compound **13** has low membrane retention with an R value less than 0.30. Table 10 summarizes MIC, Clog P, solubility, permeability and membrane retention of clofazimine and the synthesized analogs.

Table 10. A summary of MIC, Clog P, solubility, P_e , and fraction retained in the membrane (R) for clofazimine and the synthesized analogs.

Compound	R ₁	R ₂	MIC ($\mu\text{g/mL}$)	Clog P	Solubility ($\mu\text{g/mL}$)	$P_e \times 10^{-3}$ (cm/s)	R
clofazimine	isopropyl	4-chlorophenyl	< 0.2	7.8	1.47	< 0.88**	> 0.997**
11	H	4-chlorophenyl	0.8	5.8	1.48	1.26	0.950
12	H	2-hydroxy-3-pyridyl	100	4.2	15.28	< 45.45**	> 0.144**
13	H	3-pyridyl	0.8	4.4	3.66	65.27	0.299
14	isopropyl	4-chlorophenyl	25	7.2	1.29	3.55	0.979

15	isopropyl	2-hydroxy-3-pyridyl	50	5.6	11.96	24.48	0.656
16	Isopropyl	3-pyridyl	< 0.2	5.7	2.9	12.91	0.749

The results show that there is no correlation between potency and log P. Specifically, compound **13** has a lower Clog P value and higher potency than compounds **14** and **15**, however, compound **11** has higher Clog P and higher potency than compound **12**. A compound can be potent if it has the preferred functional groups no matter what the Clog P value is. This means that it is possible to have active anti-TB agents with desired Clog P values.

On the other hand, Clog P also does not directly impact the solubility. Compound **15**, for example, has higher log P and higher solubility than compound **13**. Also, clofazimine and compound **11** have almost the same solubility, while their log P values differ by two units. Solubility of the compound in biological fluids depends on the functional groups in its structure rather than its lipophilicity.

In general, the analogs that have lower log P values tend to have better permeability. However, compound **11** has a lower log P and lower permeability than compound **14**. Thus, the permeability depends on the functional groups in the structure more than the lipophilicity of the molecule. On the other hand, Figure 23 shows that there is a correlation between log P and membrane retention. The lower the log P the lower the membrane retention is. Membrane retention is the only property that is affected by log P.

Activity, solubility and permeability are slightly affected by log P and they are affected by the structural features of the compound rather than its lipophilicity.

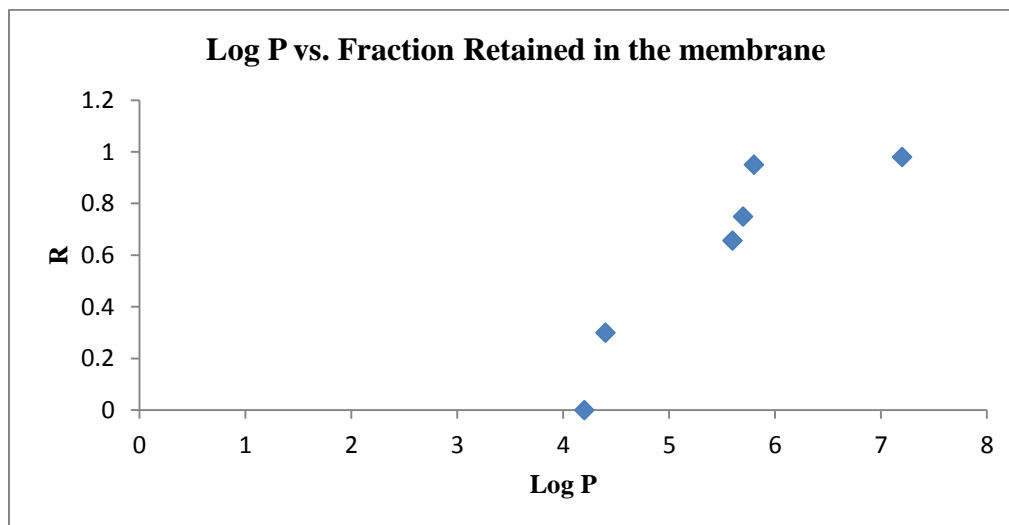


Figure 23. The correlation between log P and membrane retention.

The data show that increasing the solubility increases permeability up to a certain point. For example, compound **14** has a solubility of 3.66 $\mu\text{g/mL}$ and has the highest permeability. Solubility values of greater than 3.66 $\mu\text{g/mL}$ has a negative impact on the *in vitro* permeability. This can be justified by the need for solubility to solubilize the compounds. However, when the solubility gets higher, the compound prefers to stay in the aqueous media rather than partition through the lipophilic membrane. Increasing the solubility decreases the compound retention in the membrane because when the compound is water soluble, it has a lower tendency to dissolve in the lipophilic membrane. However, compound **15** unexpectedly has a higher solubility and a higher percent retained in the membrane than compound **13**.

Moreover, Figure 24 shows that compounds with higher permeability have lower membrane retention because they permeate through the membrane to the acceptor compartment and do not stay in the membrane.

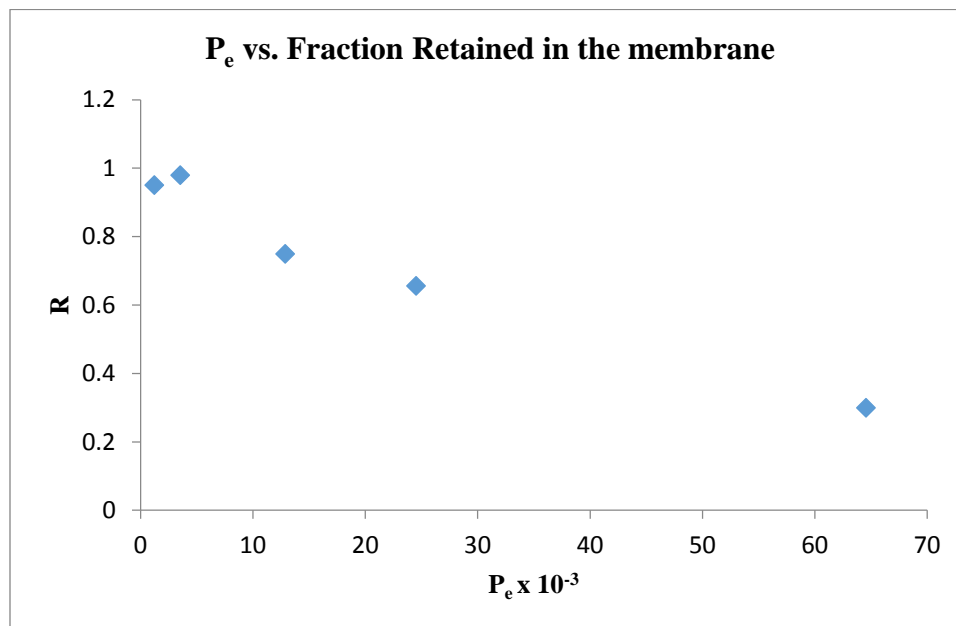


Figure 24. Compounds permeability vs. their retention in the membrane.

3.7 Experimental

3.7.1 Materials and instrumentation

All chemicals, solvents, and glassware were purchased from either Fisher Scientific (Pittsburg, Pennsylvania) or Sigma Aldrich (St. Louis, Missouri). Waters Acquity Ultra Performance LCTM was used for quantification. An Acquity UPLC[®] system (Waters Corporation, Milford, MA) equipped with a HSS T3 (1.8 μ m) 2.1 X 100 mm column and a mobile phase of 26 : 74 10 mM citrate buffer : methanol was used at a 0.40 mL/min

flow rate. UV absorbance (monitored at 286 and 492 nm) was used for detection of analytes. Permeability assay was performed using the Millipore Corporation (Billerica, MA) MultiScreen-IP PAMPA assay plates (cat. MAIPN4550), with 0.28 cm² filters (20% porosity), and PTFE acceptor plates (cat. MATRNPS50) and their standard operating procedures. The QikProp module (Schrödinger LLC) was used for Clog P calculation.

3.7.2 UPLC quantification method validation

A stock solution of clofazimine (1 mg/mL) in mobile phase was prepared and diluted to 0.1, 10, 20, and 40 µg/mL. For accuracy, the mean of the detected concentrations of five injections for each concentration was compared with the theoretical concentration, and they were all within 6% of the theoretical concentration. For intra-day precision, five injections for each concentration were done in the same day, and the coefficient of variance was found to be less than 5% for all of the concentrations. For inter-day precision, fifteen injections for each concentration were done in 3 different days (5 injections per day), and the coefficient of variance was found to be less than 5% for all of the concentrations.

3.7.3 MIC determination

A microbroth dilution method was used in accordance with the CLSI.⁷⁶ DMSO stock of each compound (10 mg/mL) was prepared and serially diluted with Middlebrook 7H9 media. A 100 µL of each dilution was transferred to a 96-well round bottom microtitre plate. *M. tuberculosis* H37Rv was grown in Middlebrook 7H9 media with 0.05% Tween 80 at 37 °C. To each well, 100 µL (10⁴ cfu) of the culture was added giving a final volume of 200 µL and a drug concentration range of 0.2 – 200 µg/mL. The plates were

incubated at 37 °C for 7 days, and the minimum concentration of compound that inhibits >90% of bacterial growth (MIC) was determined by visual inspection.

2.7.4 Thermodynamic solubility determination

Excess amount of clofazimine was added to water, citrate buffer, acetate buffer, hexane, methanol, ethanol, acetonitrile, methylene chloride and octanol in a 20 mL scintillation vial to form two different phases, a liquid and a solid phase. The mixtures were incubated at 37 °C with agitation for 72 hours. After incubation, the samples were centrifuged and 1 mL of the supernatant in each sample was dried under a stream of nitrogen gas and reconstituted and sonicated in 1 mL mobile phase. The concentrations were determined using clofazimine standard curve 286 nm (Figure 19) using the liquid chromatography quantification method described in the materials and instrumentation section.

3.7.5 Kinetic solubility determination

Compounds initially were dissolved in DMSO at a final concentration of 10 mg/mL. The stock solution was diluted with 1% DMSO in simulated lung fluid (SLF)⁷⁷ to give a final concentration of 100 µg/mL, and incubated at 37 °C for 72 h in a sealed vial. After incubation, the samples were centrifuged and 0.5 mL of the supernatant in each sample was dried under a stream of nitrogen gas and reconstituted and sonicated in 1 mL mobile phase for 5 minutes. Since clofazimine was able to stay suspended in the supernatant after centrifugation, centrifugation process was repeated twice for clofazimine. The concentrations were determined using calibration curves with appropriate dilution of samples with a concentration range of 0.75 – 50.00 µg/mL. Compounds were tested in

triplicate and quantified by UV spectroscopy (286 nm) using the liquid chromatography quantification method described in the materials and instrumentation section.

3.7.6 Permeability determination

A 1% solution of lecithin in dodecane was prepared and sonicated to ensure complete dissolution. The PAMPA membrane was generated by adding 5 μL of the 1% lecithin in dodecane solution to each filter. Compound solutions were prepared to a final concentration of 12.5 $\mu\text{g}/\text{mL}$ containing 50 $\mu\text{g}/\text{mL}$ of Lucifer yellow in 5% DMSO in phosphate buffered saline (PBS). To each well of the donor plate (top), 150 μL of compound solution was added ($N = 4$). To each well of the acceptor plate (bottom), 300 μL of 5% DMSO in PBS was added. The drug-filled donor plate was placed into the acceptor plate ensuring the underside of the membrane was in contact with the solution in the acceptor plate. Sealing tape was placed on the top of the donor plate and incubated for 16 hours at 37 $^{\circ}\text{C}$. After incubation, 100 μL aliquots from each well in the donor plate and 200 μL aliquots from each well in the acceptor plate were taken, the solvent was evaporated under a stream of N_2 gas, and reconstituted with 200 μL of mobile phase. The absorbance was detected at 286 nm using UPLC quantification method. To determine the drug equilibrium concentration, 150 μL of the donor plate solution and 300 μL of the acceptor plate solution were mixed. The solvent was evaporated under a stream of N_2 gas, and reconstituted with 450 μL of mobile phase. The concentrations were determined using a seven-point calibration with appropriate dilution of samples with a concentration range of 0.01 – 12.50 $\mu\text{g}/\text{mL}$.

Chapter 4

Conclusion and future perspectives

4.1 Conclusion

Replacing the lipophilic scaffold of clofazimine with a more polar three-ring core in addition to substitutions to R₁ and R₂ was able to maintain the anti-TB activity while improving solubility and permeability of the analogs. Additionally, changes to the three-ring core led to the discovery of a patentable class of novel structures for further explorations into new anti-TB agents.

Compounds **11**, **13** and **16** were potent with MIC values $\leq 0.8 \mu\text{g/mL}$, suggesting that the new scaffold is active and it is worth to pursue the characterization of the synthesized compounds. The three potent compounds have log P values at least two units less than clofazimine's log P. The solubility of the most active compounds, **11**, **13** and **16**, was not substantially improved, with compound **13** having the highest solubility of $3.66 \mu\text{g/mL}$. However, the less potent compounds **12** and **15** have significantly improved solubility. It is apparent that when the solubility is increased, TB compounds start losing their activity and, therefore, TB activity and solubility have an inverse relationship.

Compound **13** not only has the highest solubility, it also has the highest permeability, with a P_e value of $65.27 \times 10^{-3} \text{ cm/s}$, and the lowest fraction retained in the membrane, with a R-value of 0.299. Higher permeability and lower membrane retention mean that the compounds are able to cross the lipophilic biological membrane with a decreased propensity of lipid accumulation.

Compound **13** is the compound that is potent and has the lowest log P value, the highest solubility and permeability, and the lowest R-value among the potent compound. Thus, compound **13** is considered the most promising of the six synthesized compounds.

Improvement of the aqueous solubility and membrane permeability of compound **13** should then eventually lead to toxicity reduction and pharmacokinetic properties improvement compared to clofazimine. Specifically, compound **13** might potentially have lower accumulation tendency in skin, organs and adipose tissue. Since clofazimine accumulation causes skin and conjunctiva discoloration, compounds with lower accumulation are anticipated to have lower discoloration. Compound **11**, for example, is a brown compound and it has an R value of 0.95, and it is anticipated to accumulate in the skin causing the undesired discoloration. On the other hand, although compound **13** is also a brown compound, it has an R value of 0.299, and it is anticipated to have a decreased skin discoloration because it has the ability to permeate through the lipophilic membranes leaving a very small fraction of its molecules in the membranes and lipophilic tissues.

Also, GI toxicity is caused by clofazimine accumulation in the epithelial cells in the GI tract. Having an anticipated lower accumulation propensity of compound **13** is expected to decrease the GI irritation experienced following clofazimine exposure. Lower skin and conjunctiva discoloration and GI irritation of compound **13** are anticipated to increase the patient compliance and, therefore, have an increased effectiveness in TB management.

Compound **13** is anticipated to have a different distribution pattern. After absorption, clofazimine instantaneously leaves the blood and is stored in body organs resulting in a huge volume of distribution of 1470 L.⁵⁰ However, compound **13** is expected to have a smaller volume of distribution, since it should have a lower tendency to accumulate in body organs.

Moreover, it is expected that compound **13** will have a shorter half-life. The removal of the chlorine atom in the E ring makes the aromatic ring vulnerable for aromatic hydroxylation in phase I liver metabolism. The reduced volume of distribution and the shorter half-life are clinical signs for the improved pharmacokinetic properties and decreased drug accumulation, which consequently leads to lower toxicity and side effects.

4.2 Global Perspectives

As stated earlier, TB is a global epidemic where the resistant strains are ever increasing. The discovery of new promising leads, such as compound **13**, for TB treatment is the first step in the battle to eliminate TB worldwide. The discovery and subsequent *in vitro* testing of lead compounds is important to establish the base for the pre-clinical and the clinical studies. Further, the approval of a new anti-TB agent that has the ideal properties should then lead to improved quality of life and ultimately cure patients infected with resistant strains of *M. tuberculosis*. Consequently, the sustained discovery of new anti-TB agents can also result in a completely novel treatment regimen that should decrease the number of resistant TB cases, the number of TB deaths and, eventually, end TB.

4.3 Future perspectives

4.3.1 Synthetic scheme optimization and synthesis of more compounds

The reaction scheme for the analog synthesis needs further optimization to improve the yields for the low yielding reduction reactions. For example, the use of zinc instead of iron for the reduction of the nitro groups might be able to improve the reaction yield.

Moreover, negatively charged nucleophiles are stronger since they have extra electrons and they want to share them with an electrophile in order to return back to the more stable neutral state. Therefore, the use of carbanionic reagents, such as butyl lithium, to make the nucleophiles negatively charged is a suggested way to improve the yields of nucleophilic aromatic substitution reactions and to utilize the weaker nucleophiles as potential substituents.

With six compounds synthesized and tested, discernable and predictable SAR is forming. However, more compounds are needed to build the SAR for the new scaffold. Changing the R₂ substituent had a good impact on activity and pharmacokinetic properties, and the addition of a nitrogen atom in the E ring had the most potent activity and the best pharmacokinetic parameters. Therefore, a list of nitrogen containing E rings is suggested (Figure 25), which will also further establish the current SAR. The addition of hydroxyl group diminishes activity. However, the presence of the oxygen improves the solubility and log P. Accordingly, some rings in the suggested list contain ether groups rather than hydroxyl groups. The addition of the ether is anticipated to maintain activity and improve the pharmacokinetic properties.

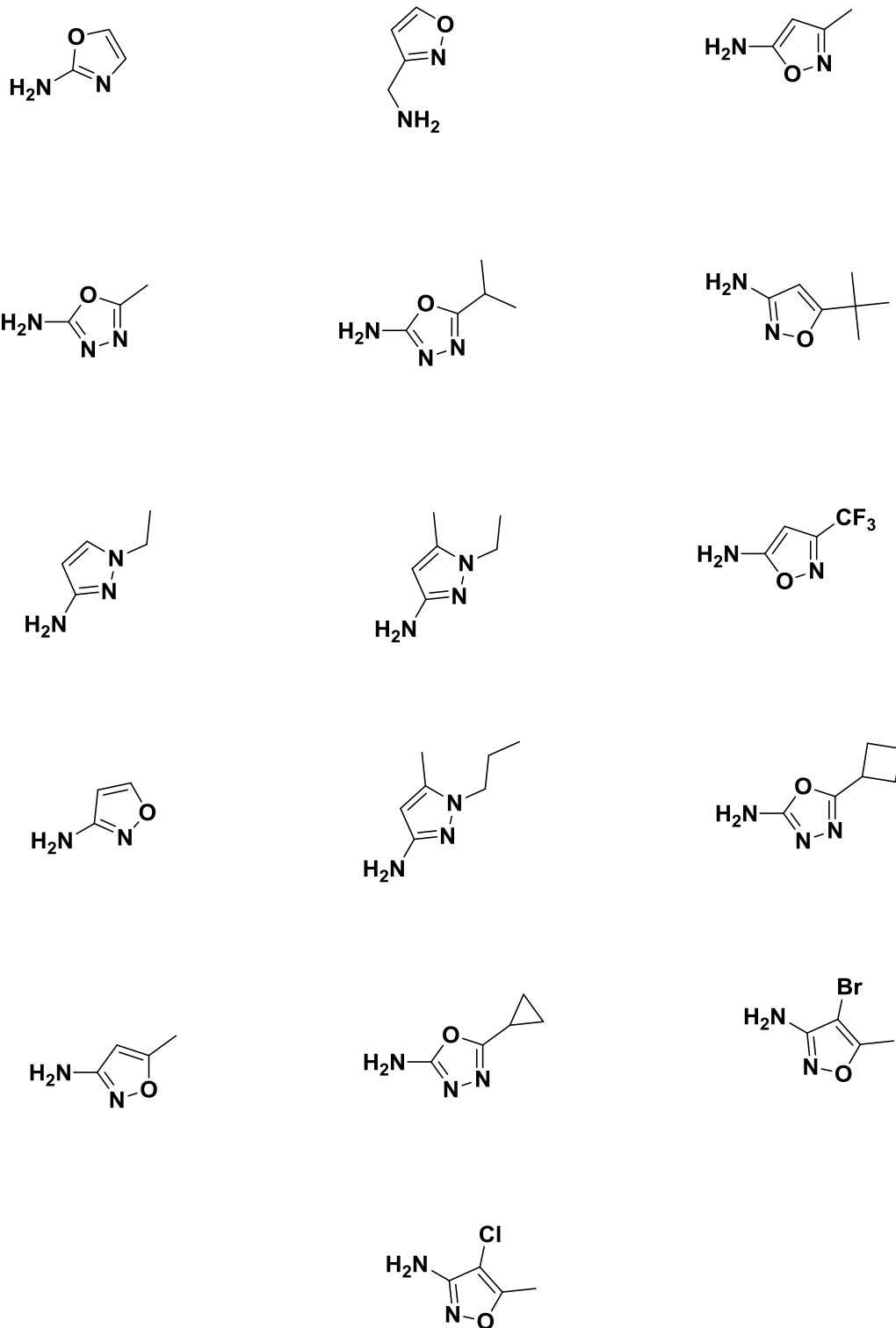


Figure 25. Potential substituents for ring E

Since the new scaffold was active and a nitrogen is tolerated in the A ring, other scaffolds should be explored. For example, changing the position and the number of the new nitrogen atoms in the A ring (Figure 26) might result in potential new active scaffolds.

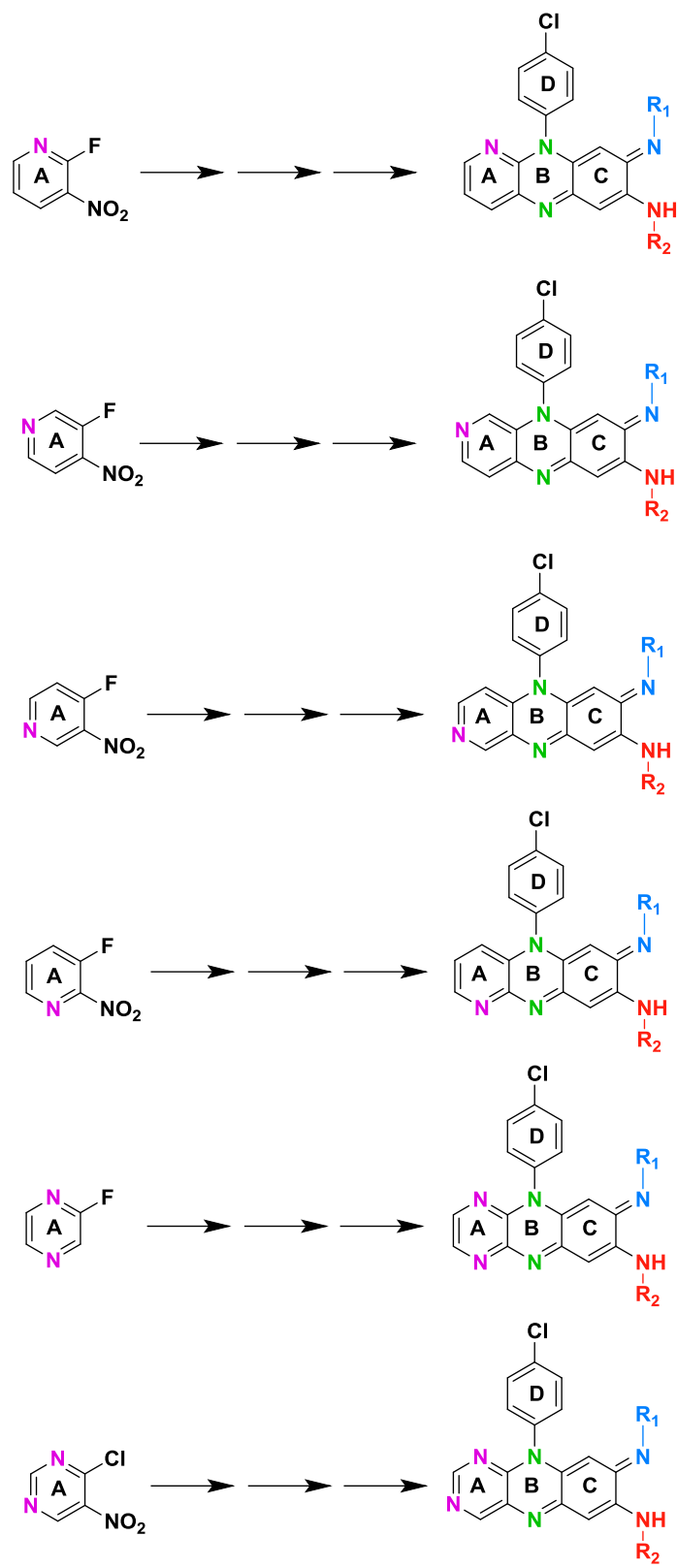


Figure26. Further A ring modifications.

New scaffold synthesis can be accomplished simply by changing the starting material with the use of the same reaction scheme (Scheme 1). All of the starting materials shown in Figure 23 are commercially available from either Fisher Scientific (Pittsburg, Pennsylvania) or Sigma Aldrich (St. Louis, Missouri).

4.3.2 Efficacy and pharmacokinetic studies compound 13

As compound **13** has a good *in vitro* activity and improved pharmacokinetic proxy measures, cytotoxicity, human plasma protein binding, microsomal stability are other suggested *in vitro* ADME-toxicity properties helping to predict the PK/PD. Moreover, compound **13** is promising and warrants further investigation with its *in vitro* intracellular activity, *in vivo* safety and pharmacokinetic properties and *in vivo* efficacy.

4.3.2.1 *In vitro* intracellular activity study design

After infection, mycobacteria are found in the macrophages in the well-ventilated human lungs and are classified as facultative intracellular parasites.⁷⁸ Thus, for a drug to be active it must have the ability to penetrate macrophages and reach the bacilli.

The intracellular activity assay is usually done if the compound is active in the microbroth dilution method (Section 3.7.3), in order to simulate the actual infection and indicate the ability of the anti-TB agent to inhibit the intracellular bacilli inside the human body.

4.3.2.3 *In vivo* safety and pharmacokinetic testing study design

Monitoring the mice psychological and physiologic functions provides an idea about the type of adverse effects expected in humans. Further, the determination of organ weights is meant to address the safety profile of the drug. An increase in organ weights suggests that the drug is either accumulating in body organs or causing fluid retention, and they are both safety issues in humans.

Moreover, the improved distribution can be confirmed by measuring the concentration of compound **13** in different mice organ homogenates. Studies have reported liquid-liquid extraction methods that used methylene chloride as the organic solvent to extract clofazimine from biological samples.^{79,80} The resulting concentrations are expected to be lower than those measured for clofazimine.

4.3.2.2 *In vivo* efficacy study design

An aerosol model for acute infection should be used for preliminary *in vivo* efficacy analysis. As compound **13** passes the cell-mediated studies and we have a feel of its activity and toxicity, it is the lead compound for future animal studies. It is reported that inhaled clofazimine demonstrated *in vivo* efficacy in mice TB models.⁸¹ Thus, the inhalation route is suggested along with the oral lavage in order to compare the effect of different routes of administration and, therefore, provide a preliminary data about the efficiency of each route.

Knowing the MIC is important for dose determination. The administered dose is the dose required to keep the concentration inside the macrophages higher than the MIC. However, the dose should be modified to keep the concentration in the extracellular fluid

less than the IC_{50} . Thus, potency, toxicity and pharmacokinetic properties are major factors for dose determination. Also, the inhalation route is expected to decrease the dose required for pulmonary TB treatment since the drug is directly administered into the site of action and is not exposed to the first pass effect of the liver.

If the mean log value of the bacilli counts for the treated group is significantly lower than that for the negative-control group, with a P value of ≤ 0.05 , compound **13** is considered effective in an infected mouse model of TB. On the other hand, if the mean log value of the bacilli counts for the inhalation route was significantly lower than that for the oral route, with a P value of ≤ 0.05 , the inhalation route is considered more effective in mouse model for TB.

References

1. MC R, DE S, Jr, Kochi A. Global epidemiology of tuberculosis: Morbidity and mortality of a worldwide epidemic. *JAMA*. 1995;273(3):220-226.
<http://dx.doi.org/10.1001/jama.1995.03520270054031>.
2. Lewandowski CM, Co-investigator N, Lewandowski CM. WHO Global tuberculosis report 2015. *Eff Br mindfulness Interv acute pain Exp An Exam Individ Differ*. 2015;1:1689-1699. doi:10.1017/CBO9781107415324.004.
3. Jackson BR, Salter M, Tarr C, et al. Notes from the field: listeriosis associated with stone fruit - United States, 2014. *MMWR Morb Mortal Wkly Rep*. 2015;64(10):282-283. <http://www.ncbi.nlm.nih.gov/pubmed/25789745>.
4. Gradmann C. Robert Koch and the white death: from tuberculosis to tuberculin. *Microbes Infect*. 2006;8(1):294-301. doi:10.1016/j.micinf.2005.06.004.
5. Jones-Lopez EC, Namugga O, Mumbowa F, et al. Cough aerosols of *Mycobacterium tuberculosis* predict new infection: a household contact study. *Am J Respir Crit Care Med*. 2013;187(9):1007-1015. doi:10.1164/rccm.201208-1422OC.
6. Akaki T, Tomioka H, Shimizu T, Dekio S, Sato K. Comparative roles of free fatty acids with reactive nitrogen intermediates and reactive oxygen intermediates in expression of the anti-microbial activity of macrophages against *Mycobacterium tuberculosis*. *Clin Exp Immunol*. 2000;121(2):302-310.
7. Manganelli R, Provvedi R, Rodrigue S, et al. Sigma factors and global gene

- regulation in *Mycobacterium tuberculosis*. *J Bacteriol.* 2004;186(4):895-902.
doi:10.1128/JB.186.4.895.
8. Pawlowski A, Jansson M, Sköld M, Rottenberg ME, Källenius G. Tuberculosis and HIV co-infection. *PLoS Pathog.* 2012;8(2). doi:10.1371/journal.ppat.1002464.
 9. Cole ST, Brosch R, Parkhill J, et al. Deciphering the biology of *Mycobacterium tuberculosis* from the complete genome sequence. *Nature.* 1998;393(6685):537-544. doi:10.1038/31159.
 10. CDC - Centers for disease control and prevention. Core Curriculum on Tuberculosis, Chapter 2: Transmission and Pathogenesis of Tuberculosis. 6 Ed. 2013:19-44. doi:10.1038/ng.2747.
 11. Smith I. *Mycobacterium tuberculosis* pathogenesis and molecular determinants of virulence. *Clin Microbiol Rev.* 2003;16(3):463-496.
 12. Daffe M, Etienne G. The capsule of *Mycobacterium tuberculosis* and its implications for pathogenicity. *Tuber Lung Dis.* 1999;79(3):153-169.
doi:10.1054/tuld.1998.0200.
 13. Andersen P, Doherty TM, Pai M, Weldingh K. The prognosis of latent tuberculosis: can disease be predicted? *Trends Mol Med.* 2007;13(5):175-182.
doi:10.1016/j.molmed.2007.03.004.
 14. Schaberg T, Rebhan K, Lode H. Risk factors for side-effects of isoniazid, rifampin and pyrazinamide in patients hospitalized for pulmonary tuberculosis. *Eur Respir J.* 1996;9(10):2026-2030. doi:10.1183/09031936.96.09102026.

15. Knight GM, Gomez GB, Dodd PJ, et al. The Impact and Cost-Effectiveness of a Four-Month Regimen for First-Line Treatment of Active Tuberculosis in South Africa. *PLoS One*. 2015;10(12):e0145796. doi:10.1371/journal.pone.0145796.
16. Ronacher K, Joosten SA, van Crevel R, Dockrell HM, Walzl G, Ottenhoff THM. Acquired immunodeficiencies and tuberculosis: Focus on HIV/AIDS and diabetes mellitus. *Immunol Rev*. 2015;264(1):121-137. doi:10.1111/imr.12257.
17. Zohar M, Moshe L, Daniel C, Noa C, Itamar G. HIV prevalence in the Israeli tuberculosis cohort, 1999-2011. *BMC Public Health*. 2014;14:1090. doi:10.1186/1471-2458-14-1090.
18. Mekonnen D, Derbie A, Desalegn E. TB/HIV co-infections and associated factors among patients on directly observed treatment short course in Northeastern Ethiopia: a 4 years retrospective study. *BMC Res Notes*. 2015;8:666. doi:10.1186/s13104-015-1664-0.
19. Drobniewski F, Cooke M, Jordan J, et al. Systematic review, meta-analysis and economic modelling of molecular diagnostic tests for antibiotic resistance in tuberculosis. *Health Technol Assess (Rockv)*. 2015;19(34):1-188. doi:10.3310/hta19340.
20. Levy SB. The 2000 Garrod lecture. Factors impacting on the problem of antibiotic resistance. *J Antimicrob Chemother*. 2002;49(1):25-30. doi:10.1093/jac/49.1.25.
21. Levy SB, Marshall B. Antibacterial resistance worldwide: causes, challenges and responses. *NatMed*. 2004;10(1078-8956 (Print)):S122-S129. doi:10.1038/nm1145.

22. Migliori GB, Sotgiu G, D'Ambrosio L, et al. TB and MDR/XDR-TB in European Union and European Economic Area countries: Managed or mismanaged? *Eur Respir J*. 2012;39(3):619-625. doi:10.1183/09031936.00170411.
23. Olson S, English R, Claiborne A. *The New Profile of Drug-Resistant Tuberculosis in Russia : A Global and Local Perspective.*; 2011.
24. Zumla A, Nahid P, Cole ST. Advances in the development of new tuberculosis drugs and treatment regimens. *Nat Rev Drug Discov*. 2013;12(5):388-404. <http://dx.doi.org/10.1038/nrd4001>.
25. Wong EB, Cohen KA, Bishai WR. Rising to the challenge: new therapies for tuberculosis. *Trends Microbiol*. 2013;21(9):493-501. doi:10.1016/j.tim.2013.05.002.
26. Hoffmann H, Kohl TA, Hofmann-Thiel S, et al. Delamanid and Bedaquiline Resistance in Mycobacterium tuberculosis Ancestral Beijing Genotype Causing Extensively Drug-Resistant Tuberculosis in a Tibetan Refugee. *Am J Respir Crit Care Med*. 2016;193(3):337-340. doi:10.1164/rccm.201502-0372LE.
27. Bonnet M, Bastard M, du Cros P, et al. Identification of patients who could benefit from bedaquiline or delamanid: a multisite MDR-TB cohort study. *Int J Tuberc Lung Dis*. 2016;20(2):177-186. doi:10.5588/ijtld.15.0962.
28. Castro KG, Lobue P. Bridging implementation, knowledge, and ambition gaps to eliminate tuberculosis in the united states and globally. *Emerg Infect Dis*. 2011;17(3):337-342. doi:10.3201/eid1703.110031.

29. Shehzad A, Rehman G, Ul-Islam M, Khattak WA, Lee YS. Challenges in the development of drugs for the treatment of tuberculosis. *Braz J Infect Dis*. 2013;17(1):74-81. doi:10.1016/j.bjid.2012.10.009.
30. Diacon AH, Pym A, Grobusch MP, et al. Multidrug-Resistant Tuberculosis and Culture Conversion with Bedaquiline. *N Engl J Med*. 2014;371(8):723-732. doi:10.1056/NEJMoa1313865.
31. Diacon AH, Donald PR, Pym A, et al. Randomized pilot trial of eight weeks of bedaquiline (TMC207) treatment for multidrug-resistant tuberculosis: Long-term outcome, tolerability, and effect on emergence of drug resistance. *Antimicrob Agents Chemother*. 2012;56(6):3271-3276. doi:10.1128/AAC.06126-11.
32. Pym AS, Diacon AH, Tang S, et al. Bedaquiline in the treatment of multidrug- and extensively drug-resistant tuberculosis. *Eur Respir J*. 2015:ERJ - 00724-02015. doi:10.1183/13993003.00724-2015.
33. Villemagne B, Crauste C, Flipo M, Baulard AR, Déprez B, Willand N. Tuberculosis: the drug development pipeline at a glance. *Eur J Med Chem*. 2012;51:1-16. doi:10.1016/j.ejmech.2012.02.033.
34. Cabrera-rivero JL, Vargas-vasquez DE, Gao M, et al. New England Journal. 2012:2151-2160. doi:10.1056/NEJMoa1201637.
35. Skripconoka V, Danilovits M, Pehme L, et al. Delamanid improves outcomes and reduces mortality in multidrug-resistant tuberculosis. *Eur Respir J*. 2013;41(6):1393-1400. doi:10.1183/09031936.00125812.

36. Gupta R, Gao M, Cirule A, Xiao H, Geiter LJ, Wells CD. Delamanid for Extensively Drug-Resistant Tuberculosis. *N Engl J Med.* 2015;373(3):291-292. doi:10.1056/NEJMc1415332.
37. PA-824 Kills Nonreplicating. *Science (80-).* 2008;322(November):1392-1395. doi:10.1126/science.1164571.
38. Somasundaram S, Anand RS, Venkatesan P, Paramasivan CN. Bactericidal activity of PA-824 against *Mycobacterium tuberculosis* under anaerobic conditions and computational analysis of its novel analogues against mutant Ddn receptor. *BMC Microbiol.* 2013;13(1):218. doi:10.1186/1471-2180-13-218.
39. Diacon AH, Dawson R, Du Bois J, et al. Phase II dose-ranging trial of the early bactericidal activity of PA-824. *Antimicrob Agents Chemother.* 2012;56(6):3027-3031. doi:10.1128/AAC.06125-11.
40. Farah SI, Abdelrahman AA, North EJ, Chauhan H. Opportunities and Challenges for Natural Products as Novel Antituberculosis Agents. *Assay Drug Dev Technol.* 2016;14(1):29-38. doi:10.1089/adt.2015.673.
41. Palomino JC, Martin A. Is repositioning of drugs a viable alternative in the treatment of tuberculosis? *J Antimicrob Chemother.* 2013;68(2):275-283. doi:10.1093/jac/dks405.
42. Earla P. Long Lasting Disease : Leprosy. 2015;3(2):3-6. doi:10.4172/2332-0877.R1-001.
43. Zhang Z, Li T, Qu G, Pang Y, Zhao Y. In vitro synergistic activity of clofazimine

and other antituberculous drugs against multidrug-resistant Mycobacterium tuberculosis isolates. *Int J Antimicrob Agents*. 2015;45(1):71-75.
doi:10.1016/j.ijantimicag.2014.09.012.

44. Zhang D, Lu Y, Liu K, et al. Identification of less lipophilic riminophenazine derivatives for the treatment of drug-resistant tuberculosis. *J Med Chem*. 2012;55(19):8409-8417. doi:10.1021/jm300828h.
45. Brennan PJ, Young DB, Alliance G. Handbook of Anti-Tuberculosis Agents. *Tuberculosis*. 2008;88(2):85-170.
46. Liu B, Liu K, Lu Y, et al. Systematic evaluation of structure-activity relationships of the riminophenazine class and discovery of a C2 pyridylamino series for the treatment of multidrug-resistant tuberculosis. *Molecules*. 2012;17(4):4545-4559. doi:10.3390/molecules17044545.
47. Cholo MC, Steel HC, Fourie PB, Germishuizen WA, Anderson R. Clofazimine: current status and future prospects. *J Antimicrob Chemother*. 2012;67(2):290-298. doi:10.1093/jac/dkr444.
48. COSTA QUEIROZ R. BIOCHEMICAL AND HEMATOLOGICAL SIDE EFFECTS OF CLOFAZIMINE IN LEPROSY PATIENTS. *Pharmacol Res*. 2002;46(2):191-194. doi:10.1016/S1043-6618(02)00086-5.
49. Dey T, Brigden G, Cox H, Shubber Z, Cooke G, Ford N. Outcomes of clofazimine for the treatment of drug-resistant tuberculosis: A systematic review and meta-analysis. *J Antimicrob Chemother*. 2013;68(2):284-293. doi:10.1093/jac/dks389.

50. Nix DEDE, Adam RDRD, Auclair B, Krueger TSTS, Godo PGP, Peloquin CACA. Pharmacokinetics and relative bioavailability of clofazimine in relation to food, orange juice and antacid. *Tuberculosis (Edinb)*. 2004;84(6):365-373. doi:10.1016/j.tube.2004.04.001.
51. Swanson R V, Adamson J, Moodley C, et al. Pharmacokinetics and pharmacodynamics of clofazimine in a mouse model of tuberculosis. *Antimicrob Agents Chemother*. 2015;59(6):3042-3051. doi:10.1128/AAC.00260-15.
52. Holdiness MR. Clinical pharmacokinetics of clofazimine. A review. *Clin Pharmacokinet*. 1989;16(2):74-85. doi:10.2165/00003088-198916020-00002.
53. Van Rensburg CEJ, Joone GK, O'Sullivan JF, Anderson R. Antimicrobial activities of clofazimine and B669 are mediated by lysophospholipids. *Antimicrob Agents Chemother*. 1992;36(12):2729-2735. doi:10.1128/AAC.36.12.2729.
54. Imlay J, Fridovich I. Exogenous quinones directly inhibit the respiratory NADH dehydrogenase in *Escherichia coli*. *Arch Biochem Biophys*. 1992;296(1):337-346. doi:10.1016/0003-9861(92)90581-G.
55. Malone AS, Chung Y-K, Yousef AE. Proposed mechanism of inactivating *Escherichia coli* O157:H7 by ultra-high pressure in combination with tert-butylhydroquinone. *J Appl Microbiol*. 2008;105(6):2046-2057. doi:10.1111/j.1365-2672.2008.03973.x.
56. Steel HC, Matlola NM, Anderson R. Inhibition of potassium transport and growth of mycobacteria exposed to clofazimine and B669 is associated with a calcium-

- independent increase in microbial phospholipase A2 activity. *J Antimicrob Chemother.* 1999;44(2):209-216.
57. Kagan VE. Tocopherol stabilizes membrane against phospholipase A, free fatty acids, and lysophospholipids. *Ann N Y Acad Sci.* 1989;570:121-135.
58. Morrison NE, Marley GM. the Mode of Action of Clofazimine Dna Binding Studies. *Int J Lepr.* 1976;44(1):133-134.
59. Lu Y, Zheng M, Wang B, et al. Clofazimine analogs with efficacy against experimental tuberculosis and reduced potential for accumulation. *Antimicrob Agents Chemother.* 2011;55(11):5185-5193. doi:10.1128/AAC.00699-11.
60. Zhang D, Liu Y, Zhang C, et al. Synthesis and biological evaluation of novel 2-methoxypyridylamino-substituted riminophenazine derivatives as antituberculosis agents. *Molecules.* 2014;19(4):4380-4394. doi:10.3390/molecules19044380.
61. Böhm H-J, Flohr A, Stahl M. Scaffold hopping. *Drug Discov Today Technol.* 2004;1(3):217-224. doi:10.1016/j.ddtec.2004.10.009.
62. Brown N, Jacoby E. On scaffolds and hopping in medicinal chemistry. *Mini Rev Med Chem.* 2006;6(11):1217-1229. doi:10.2174/138955706778742768.
63. Vogt M, Stumpfe D, Geppert H, Bajorath J. Scaffold hopping using two-dimensional fingerprints: True potential, black magic, or a hopeless endeavor? Guidelines for virtual screening. *J Med Chem.* 2010;53(15):5707-5715. doi:10.1021/jm100492z.
64. Teuber L, Watjens F, Jensen LH. Ligands for the benzodiazepine binding site--a

- survey. *Curr Pharm Des.* 1999;5(5):317-343.
65. Meanwell NA. Synopsis of some recent tactical application of bioisosteres in drug design. *J Med Chem.* 2011;54(8):2529-2591. doi:10.1021/jm1013693.
66. Matta CF, Arabi AA, Weaver DF. The bioisosteric similarity of the tetrazole and carboxylate anions: clues from the topologies of the electrostatic potential and of the electron density. *Eur J Med Chem.* 2010;45(5):1868-1872.
doi:10.1016/j.ejmech.2010.01.025.
67. Ertl P. In silico identification of bioisosteric functional groups. *Curr Opin Drug Discov Devel.* 2007;10(3):281-288.
68. Liu B, Liu K, Lu Y, et al. Systematic evaluation of structure-activity relationships of the riminophenazine class and discovery of a C2 pyridylamino series for the treatment of multidrug-resistant tuberculosis. *Molecules.* 2012;17(4):4545-4559.
doi:10.3390/molecules17044545.
69. Lakshminarayana SB, Huat TB, Ho PC, et al. Comprehensive physicochemical, pharmacokinetic and activity profiling of anti-TB agents. *J Antimicrob Chemother.* 2015;70(3):857-867. doi:10.1093/jac/dku457.
70. Food and Drug Administration. Guidance for industry. Bioanalytical method validation. 2013;(September).
<http://www.fda.gov/downloads/drugs/guidancecomplianceregulatoryinformation/guidances/ucm368107.pdf>.
71. Wang J, Wang J, Urban L, Urban L. The impact of early ADME profiling on drug

- discovery and development strategy. *Drug Discov World*. 2004:73-86.
72. Bermejo M, Avdeef A, Ruiz A, et al. PAMPA--a drug absorption in vitro model 7. Comparing rat in situ, Caco-2, and PAMPA permeability of fluoroquinolones. *Eur J Pharm Sci*. 2004;21(4):429-441. doi:10.1016/j.ejps.2003.10.009.
73. Membrane A, Assays P. MultiScreen Filter Plates for PAMPA. *Small*.
74. Wohnsland F, Faller B. High-throughput permeability pH profile and high-throughput alkane/water log P with artificial membranes. *J Med Chem*. 2001;44(6):923-930. doi:10.1021/jm001020e.
75. Markovic BD, Vladimirov SM, Cudina OA, Odovic J V., Karljikovic-Rajic KD. A PAMPA assay as fast predictive model of passive human skin permeability of new synthesized corticosteroid C-21 esters. *Molecules*. 2012;17(1):480-491. doi:10.3390/molecules17010480.
76. Hurdle JG, Lee RB, Budha NR, et al. A microbiological assessment of novel nitrofuranylamides as anti-tuberculosis agents. *J Antimicrob Chemother*. 2008;62(5):1037-1045. doi:10.1093/jac/dkn307.
77. Marques MRC, Loebenberg R, Almukainzi M. Simulated biological fluids with possible application in dissolution testing. *Dissolution Technol*. 2011;18(3):15-28. doi:10.1002/jps.23029.
78. Leon-Sicairos N, Reyes-Cortes R, Guadr??n-Llanos AM, Madue??a-Molina J, Leon-Sicairos C, Canizalez-Rom??n A. Strategies of intracellular pathogens for obtaining iron from the environment. *Biomed Res Int*. 2015;2015.

doi:10.1155/2015/476534.

79. O'Connor R, O'Sullivan JF, O'Kennedy R. Determination of serum and tissue levels of phenazines including clofazimine. *J Chromatogr B Biomed Sci Appl.* 1996;681(2):307-315. doi:10.1016/0378-4347(96)00025-4.
80. Baik J, Stringer KA, Mane G, Rosania GR. Multiscale distribution and bioaccumulation analysis of clofazimine reveals a massive immune system-mediated xenobiotic sequestration response. *Antimicrob Agents Chemother.* 2013;57(3):1218-1230. doi:10.1128/AAC.01731-12.
81. Verma RK, Germishuizen WA, Motheo MP, et al. Inhaled microparticles containing clofazimine are efficacious in treatment of experimental tuberculosis in mice. *Antimicrob Agents Chemother.* 2013;57(2):1050-1052. doi:10.1128/AAC.01897-12.